Prediction Of Geospace Radiation Environment and Solar wind parameterS

Work Package 5
Low energy electrons model improvements to develop forecasting products

Deliverable D5.2
The incorporation of diffusion coefficients from VERB into IMPTAM

N. Ganushkina, S. Dubyagin, I. Sillanpää
December 31, 2016

This project has received funding from the European Union's Horizon 2020 research and innovation programme under grant agreement No 637302

Document Change Record

Issue	Date	Author	Details
v1	30.12.2016	N. Ganushkina	
v2	08.03.2017	N. Ganushkina	revision after reviewer's comments

Table of Contents

1. Introduction

The **Deliverable D5.2** entitled "The incorporation of diffusion coefficients from VERB into IMPTAM" is the second Deliverable of the **WP5** "Low energy electrons model improvements to develop forecasting products". The second objective of this WP is to adapt the IMPTAM to include proper diffusion coefficients provided by VERB radiation belts model. During the work under the Deliverable **D5.2**, the main focus was set at the **Task 5.2** "Incorporating the proper diffusion coefficients into IMPTAM provided by VERB radiation belts model".

Electrons with energies less than 100 keV are one of the important constituents of the inner Earth's magnetosphere. The electron fluxes at these keV energies vary significantly with the current activity on the scale of minutes or even shorter [*Ganushkina et al*., 2013, 2014]. Electron losses occur on the time scales of minutes or hours which is much shorter than those times for ions. The dominant loss process is pitch angle scattering with due to interactions with waves (see, for example, the reviews by *Shprits et al*. [2008a,b] and references therein) which results in the precipitation of electrons into the ionosphere. Lower band chorus (LBC) and upper band chorus (UBC) waves contribute significantly to the scattering processes of keV electrons outside the plasmapause. Inside the plasmasphere, electron pitch angle scattering occurs due to interactions with the plasmaspheric hiss. It is difficult to quantify globally the electron losses due to pitch angle scattering, since the rate of pitch angle diffusion for a given electron energy depends on the wave amplitude, wave frequency, and wave normal distributions, as well as the plasma density and background magnetic field.

Wave-particle interactions have to be incorporated into the IMPTAM model via diffusion coefficients. The proper incorporation of wave-particle interactions was possible due to the existence of Full Diffusion Code (FDC) model [*Shprits and Ni*, 2009], which provided the diffusion coefficients calculated in a non-dipole field [*Orlova et al*., 2012]. The matrix of diffusion coefficients as a function of L-shell, pitch-angle, and energy for various levels of geomagnetic activity was computed by FDC. Using the diffusion coefficients, the losses were parameterized. The model for the electron lifetimes due to interactions with chorus waves was parameterized by kinetic energy, distance, and Kp for night, dawn, prenoon, and postnoon MLT sectors [*Orlova and Shprits*, 2014]. For hiss waves, two models were developed, one based on CRRES observations [*Orlova et al*., 2014] and another on Van Allen Probes measurements [*Orlova et al*., 2016], both computed lifetimes parameterized as a function of L, kinetic energy, Kp and MLT. These computed lifetimes were included in to the IMPTAM code.

The modeling results are presented for one example storm event on February 28 - March 2, 2013. Data on low energy electron fluxes from several satellites in the inner magnetosphere were available for this storm period. We primarily used the electron fluxes with energies from 1 to 50 keV for our analysis. These energies are most important for surface charging. We focused on the results for AMC 12 measurements at geostationary orbit and for Van Allen Probes inside geostationary orbit. AMC12 CEASE electrostatic analyzer measured low energy electron fluxes in 10 channels, covering the range 5 – 50 keV. The Van Allen Probes mission consists of two spacecraft in near-equatorial elliptical orbits around Earth, traversing the inner magnetosphere at distances from 1.1 R_E to 5.8

R_E at a 9-hour period. The two satellites have slightly different orbits, with one lapping the other every 2.5 months. We use measurements from HOPE instrument which measures the pitch angle distribution of electrons over the energy range from 1 keV up to 45 keV and from MagEIS instrument with electron measurements over the energy range of 30 keV to 200 keV.

The results of data-model comparison are presented in the paper "Losses of keV electrons in the inner Earth's magnetosphere" by N. Ganushkina, I. Sillanpää, S. Dubyagin, Yu. Shprits (draft for submission), below as a part of the **Deliverable D5.2** report.

2. Conclusions

The losses are taken into account by incorporating the electron lifetimes into IMPTAM following several models. The modeling results are presented for one example storm event on February 28 - March 2, 2013. The data-model comparison are made for observations at geostationary orbit by AMC12 satellite measuring electron fluxes with energies from 5 to 50 keV and inside geostationary orbit by Van Allen Probes instruments covering the energy range from 1 to 200 keV. It was demonstrated that in the absence of electron losses, all variations which can be seen in the modeled low energy electron fluxes at geostationary orbit are caused by the variations in IMPTAM's parameters which are the solar wind and IMF parameters and Dst index included in background magnetic and electric field models and boundary conditions. The inclusion of the strong diffusion resulted in flux drops to almost zero values at and inside geostationary orbit at day- and duskside. Taking into account the electron losses by electron lifetimes for strong and weak diffusion (following *Chen et al*. [2005]), led to somewhat reasonable agreement between the observed and modeled fluxes with the modeled fluxes being one order of magnitude higher than the observed ones. The fluxes with electron energies from 15 to 50 keV are better modeled. The detailed dynamics of the observed fluxes was not reproduced. When the electron losses due to interactions with chorus waves [*Orlova and Shprits*, 2014] and with hiss waves [*Orlova et al*., 2014, 2016] were introduced, the observed geostationary electron fluxes were well reproduced during the storm maximum. The fluxes of electrons with energies from 15 to 50 keV were closer to the observed ones than those with lower energies between 5 and 15 keV. The discrepancy between the modeled and the observed fluxes is due to the way how the electron lifetimes were parameterized for low energies. Although, the detailed dynamics of observed fluxes was not fully reproduced, the representation for electron lifetimes for keV electrons obtained from the VERB code is the best available model at present. The keV electron fluxes vary significantly on the time scales of tens of minutes. The electron lifetimes parameterized by 3-hour Kp index do not reflect the full picture of shorter time variations. Further IMPTAM validation will lead to better understanding of the necessity to develop the model for electron lifetimes with more detailed dependence on energy and other than Kp geomagnetic indices.

3. Future tasks and connection to other WPs

The IMPTAM with the incorporated losses as electron lifetimes in **Deliverable D5.2** will be used further with more detailed validation throughout the project and for future Deliverables of **WP5**. Since it was shown that it is necessary to further develop the model for electron lifetimes with more detailed dependence on energy and other than Kp geomagnetic indices, the steps towards this will be taken during the work under **Task 5.3**. In **Task 5.3**, maps in (L, MLT, pitch angle, energy) of low energy electrons will be constructed as output from the improved IMPTAM. Both quiet and disturbed events will be selected for modelling according to data availability, and the model output will be compared to the observed electron fluxes to further model verification. The low energy electron maps for the modelled events will be provided to the VERB code as seed keV population for further accelerations to MeV energies. The results of the IMPTAM will be validated against satellite observations and will be also compared with the NARMAX predictions (**Task 6.3** in **WP6**). **Task 5.4** will result in developing of a trial version of forecast model for low energy electrons which will be part of **Task 7.2** in **WP7** for implementation of VERB-IMPTAM model in fusion of forecasting tools.

4. References

Chen, M. W., M. Schulz, P. C. Anderson, G. Lu, G. Germany, and M. Wuest (2005), Storm time distributions of di_use auroral electron energy and X-ray flux: Comparison of drift-loss simulations with observations, J. Geophys. Res., 110, A03210, 745 doi:10.1029/2004JA010725.

Ganushkina N. Yu., O. Amariutei, Y. Y. Shpritz, and M. Liemohn, Transport of the plasma sheet electrons to the geostationary distances, *J. Geophys. Res.*, 118, doi:10.1029/2012JA017923, 2013.

Ganushkina N. Yu., M. Liemohn, O. Amariutei, and D. Pitchford, Low energy electrons (5-50 keV) in the inner magnetosphere, *J. Geophys. Res.*, 119, 246259, 549 doi:10.1002/2013JA019304, 2014.

Orlova, K. G., Y. Y. Shprits, and B. Ni, Bounce-averaged diffusion coefficients due to resonant interaction of the outer radiation belt electrons with oblique chorus waves computed in a realistic magnetic field model, J. Geophys. Res., 117, A07209, doi:10.1029/2012JA017591, 2012.

Orlova, K., and Y. Shprits (2014), Model of lifetimes of the outer radiation belt electrons in a realistic magnetic field using realistic chorus wave parameters, J. Geophys. Res., 119, 770-780, doi:10.1002/2013JA019596.

Orlova, K., M. Spasojevic, and Y. Shprits (2014), Activity-dependent global model of electron loss inside the plasmasphere, Geophys. Res. Lett., 41, doi:10.1002/2014GL060100.

Orlova, K., Y. Shprits, and M. Spasojevic, New global loss model of energetic and relativistic electrons based on Van Allen Probes measurements, J. Geophys. Res. Space Physics, 121, 1308-1314, doi:10.1002/2015JA021878, 2016.

Shprits, Y. Y., et al., Review of modeling of losses and sources of relativistic electrons in the outer radiation belt: I. Radial transport, J. Atmos. Sol. Terr. Phys., 70(14), 1679-914 1693, 2008a.

Shprits, Y. Y., Review of modeling of losses and sources of relativistic electrons in the outer radiation belt: II. Local acceleration and loss, J. Atmos. Sol. Terr. Phys., 70(14), 1694-1713, 2008b.

Shprits, Y. Y., and B. Ni, The dependence of the quasi-linear scattering rates on the wave-normal distribution for chorus waves in the radiation belt, J. Geophys. Res., 114, A11205, doi:10.1029/2009JA014223, 2009.

Losses of keV electrons in the inner Earth's magnetosphere

N. Yu. Ganushkina[1,2], I. Sillanpaa[1], S. Dubyagin[1], Yu. Shprits[3]

[1]Finnish Meteorological Institute, Earth Observations, Helsinki, Finland.
[2]University of Michigan, Ann Arbor, Michigan, USA.
[3]Helmholtz Centre Potsdam GFZ, Potsdam, Germany.

Key Points:

- Without losses, all variations in modeled electron fluxes are due to driving parameters
- Combination of losses due to chorus and hiss waves results in best agreement between observed and modeled fluxes at geostationary orbit
- Detailed representation of electron lifetimes for below 15 keV electrons is needed

Corresponding author: N. Yu. Ganushkina, `Natalia.Ganushkina@fmi.fi`

Abstract

The role of the loss process of pitch angle diffusion for keV electrons in the inner Earth's magnetosphere is investigated. The losses are taken into account by incorporating the electron lifetimes into Inner Magnetosphere Particle Transport and Acceleration Model (IMPTAM) following several models. The modeling results are presented for one example storm event on February 28 - March 2, 2013. The data-model comparison are made for observations at geostationary orbit by AMC12 satellite measuring electron fluxes with energies from 5 to 50 keV and inside geostationary orbit by Van Allen Probes instruments covering the energy range from 1 to 200 keV. It was demonstrated that in the absence of electron losses, all variations which can be seen in the modeled low energy electron fluxes at geostationary orbit are caused by the variations in IMPTAM's parameters which are the solar wind and IMF parameters and Dst index included in background magnetic and electric field models and boundary conditions. The inclusion of the strong diffusion only (according to *Chen and Schulz* [2001b]) resulted in flux drops to almost zero values at and inside geostationary orbit at day- and duskside. Taking into account the electron losses by electron lifetimes for strong and weak diffusion (following *Chen et al*. [2005]), led to somewhat reasonable agreement between the observed and modeled fluxes with the modeled fluxes being one order of magnitude higher than the observed ones. The fluxes with electron energies from 15 to 50 keV are better modeled. The detailed dynamics of the observed fluxes was not reproduced. On the next step, instead of representing the strong and weak diffusion in general form, pitch angle diffusion due to interaction with the specific waves was introduced as the electron losses due to interactions with chorus waves [*Orlova and Shprits*, 2014] and with hiss waves [*Orlova et al.*, 2014, 2016]. The observed geostationary electron fluxes were well reproduced during the storm maximum. The fluxes of electrons with energies from 15 to 50 keV were closer to the observed ones than those with lower energies between 5 and 15 keV. The discrepancy between the modeled and the observed fluxes is due to the way how the electron lifetimes were parameterized for low energies. Although, the detailed dynamics of observed fluxes was not fully reproduced, the representation for electron lifetimes for keV electrons obtained from the VERB code is the best available model at present. The keV electron fluxes vary significantly on the time scales of tens of minutes. The electron lifetimes parameterized by 3-hour Kp index do not reflect the full picture of shorter time variations. Further IMPTAM validation will

lead to better understanding of the necessity to develop the model for electron lifetimes with more detailed dependence on energy and other than Kp geomagnetic indices.

1 Introduction

Electrons with energies less than 100 keV are one of the important constituents of the inner Earth's magnetosphere. Measurements of inner magnetosphere electrons are sparse as compared to the ions. Based on OGO 3 satellite data, it was shown that low-energy (<50 keV) electrons provide about 25% of the energy in the ring current region during storm times [*Frank*, 1967]. *Liu et al.* [2005] analyzed Explorer 45 electron data for energies from 1 to 200 keV and found the electron contribution of about 7.5% during quiet time and about 19% during storm time.

The electron fluxes at these keV energies vary significantly with the geomagnetic activity on the scale of minutes or even shorter, e.g. they react rather quickly to the activity changes. The electrons with energies of 10's of keVs do not penetrate deep into the satellite materials but stay near the surface. They can be responsible for surface charging effects which is a serious risk for satellites [*Garrett*, 1981; *Lanzerotti et al.*, 1998; *Davis et al.*, 2008].

keV electrons constitute the seed population, being further accelerated to MeV energies by various processes in the Earth's radiation belts. The acceleration process is due to interactions with the VLF whistler-mode chorus waves, which grow as a result of a presence of the anisotropic population of electrons at energies of 10's to 100's of keVs [*Helliwell*, 1967] caused by substorm injections [*Tsurutani and Smith*, 1974]. Chorus waves interact with seed electrons through cyclotron resonance and can accelerate electrons to very high energies [*Kennel and Petschek*, 1966; *Horne et al.*, 2005; *Chen et al.*, 2007; *Thorne*, 2010]. Energetic charged particles trapped in the radiation belts are a major source of damaging space weather effects on space assets.

Resonant interactions with different kind of waves in the magnetosphere violate the first or second or both adiabatic invariants of the particle motion and result in pitch angle scattering and in subsequent loss into the atmosphere (see, for example, the reviews by *Shprits et al.* [2008a,b] and references therein). Due to pitch angle scattering, equatorial pitch angle become small enough to be inside the loss cone. When the bounce-averaged pitch angle scattering rate $D_{\alpha\alpha}$ is much smaller than $4\alpha_{LC}^2/\tau_B$ (where τ_B is the bounce period for particles with equatorial pitch angle α_{LC}), the equatorial loss cone remains essentially empty. According to *Kennel* [1969] and *Schulz* [1974], the particles undergo "weak diffusion" which cannot result in efficient depletion of magnetospheric particles by diffusing the quasi-trapped population into the equatorial loss cone. Weak diffusion occurs at L-shells where particle distribution is essentially anisotropic, such as, inside the plasmasphere. When the scattering due to wave-particle interactions is rapid enough to become comparable to or above $4\alpha_{LC}^2/\tau_B$, particles diffuse across the equatorial loss cone in less than a quarter bounce period and the particle distribution can maintain an essentially filled loss cone that approaches isotropy, and this process is called "strong diffusion" [*Kennel*, 1969; *Schulz*, 1974]. Strong diffusion occurs at L-shells where the particle distribution is very close to isotropic, such as, for example, in the near-Earth plasma sheet.

Electron losses occur on the time scales of minutes or hours which is much shorter than those times for ions. Lower band chorus (LBC) and upper band chorus (UBC) waves contribute significantly to the scattering processes of keV electrons outside the plasmapause. Inside the plasmasphere, electron pitch angle scattering occurrs due to interactions with the plasmaspheric hiss [*Lyons et al.*, 1972; *Albert*, 1994] which was observed by OGO satellite series as incoherent whistler mode emissions in the ELF/VLF frequency range [*Russell et al.*, 1969; *Thorne et al.*, 1973]. It was shown that hiss waves are responsible for the formation of the slot region [*Lyons and Thorne*, 1973] in the radiation belts.

It is difficult to quantify globally the electron losses due to pitch angle scattering, since the rate of pitch angle diffusion for a given electron energy depends on the wave amplitude, wave frequency, and wave normal distributions, as well as the plasma density and background magnetic field. Earlier representation of electron lifetimes due to strong pitch angle scattering [*Schulz*, 1974, 1998] have been widely used when modeling inner magnetosphere electrons. *Chen and Schulz* [2001a,b] formulated a combination of two models for electron pitch-angle scattering, one of them corresponded to the limiting idealization of strong pitch-angle diffusion everywhere and the other was based on the "less than everywhere strong" (the term used by the authors) scattering with a prescribed dependence on MLT. This combination allowed a smooth transition from strong pitch angle diffusion in the plasma sheet to weak diffusion in the plasmasphere. Types of wave-particle interactions due to certain waves were not specified. Using of this model resulted in a good agreement between the simulated diffuse auroral electron distributions and observations [*Chen et al.*, 2005] but the disadvantage was the absence of activity dependence in the model.

Quite recently, separate parameterizations of electron lifetimes for chorus and hiss waves were developed. Several studies have recently examined the chorus wave properties [*Haque et al.*, 2010; *Li et al.*, 2011; *Ni et al.*, 2011; *Bunch et al.*, 2012; *Meredith et al.*, 2012; *Bunch et al.*, 2013; *Agapitov et al.*, 2013; *Spasojevic and Shprits*, 2013]. Earlier studies on the calculations and parameterization of the electron lifetimes due to the resonant interactions with chorus waves [*Shprits et al.*, 2007; *Gu et al.*, 2012; *Mourenas and Ripoll*, 2012; *Artemyev et al.*, 2013a] used the dipole field approximation. *Orlova and Shprits* [2014] have developed a realistic chorus wave model and calculated the electron lifetimes in the realistic Tsyganenko T89 [*Tsyganenko*, 1989] magnetic field model. The model was parameterized by kinetic energy, distance, and Kp for night, dawn, prenoon, and postnoon MLT sectors. At distances > 5 R_E, lifetimes of 10 keV electrons can be of several hours for Kp = 2 and of 15 min for Kp=6. For fixed Kp and E > 10 keV, lifetimes decrease by several times from 3 to 8 R_E. For energies < 50 keV, chorus waves contribute to electron scattering mainly at night- and dawnside. At larger energies, dominant scattering of electrons occurs on the dawn and prenoon MLT sectors.

There are number of effects which can influence the scattering rates and which are not fully understood. The wave amplitude is one of the most important factors that determine the scattering rates. Currently, the detailed chorus wave statistical properties at high latitudes are not known. *Shprits et al.* [2006] showed that the diffusion coefficients are highly dependent on the plasma density and latitudinal distribution of waves. It was recently shown that very oblique chorus waves with even small amplitude can substantially influence electron scattering and strongly reduce the lifetimes [*Mourenas et al.*, 2012; *Artemyev et al.*, 2013b]. UBC waves mainly contribute to the lifetimes of 1-10 keV electrons and their properties are still poorly known.

Plasmaspheric hiss is important for keV electrons inside the plasmapause. Statistical studies of hiss wave distributions have demonstrated that waves are present at all MLTs being more intense on the dayside, extend to latitudes above 30 degrees, and depend on geomagnetic activity *Meredith et al.* [2004]; *Golden et al.* [2012]; *Agapitov et al.* [2013]; *Li et al.* [2015]. *Orlova et al.* [2014] obtained the empirical parameterizations of wave activity and derived a parametric model of electron lifetimes based on the data from the CR-

RES mission. Recently, *Spasojevic et al.* [2015] presented an improved empirical model of plasmaspheric hiss intensity obtained using the Van Allen Probes measurements. New parameterizations of electron lifetimes was developed by *Orlova et al.* [2016] based on hiss wave intensity model of *Spasojevic et al.* [2015] and realistic spectral distributions of *Li et al.* [2015]. The computed lifetimes are parameterized as a function of L, kinetic energy, Kp, and MLT. The wave parameters used in calculations of electron lifetimes are very important. What is missing at present are the extension of hiss intensity to high latitudes and the global models of wave normal angles at different distances.

Recent attempts to incorporate electron lifetimes with the parameterizations described above to represent the losses for keV electrons when modeling their transport in the inner magnetosphere were made by *Ganushkina et al.* [2014]; *Chen et al*. [2015]. *Ganushkina et al.* [2014] used the *Chen et al*. [2005] electron lifetimes for strong diffusion and the *Shprits et al.* [2007] electron lifetimes for weak diffusion. They studied the transport and acceleration of the 5-50 keV electrons from the plasma sheet to geostationary orbit for nonstorm event on 24-30 November 2011 with emphasis on the role of isolated substorms present during this event. *Chen et al*. [2015] incorporated the parameterized electron loss rates of chorus waves using *Orlova and Shprits* [2014] outside the plasmasphere and of hiss *Orlova et al.* [2014] inside the plasmasphere for simulations of 10 August 2000 storm with RCM-E model. They showed that the Kp and MLT parameterized electron lifetimes provide much better results compared to simple and static electron loss models such as strong diffusion.

In the present paper we investigate the role of the loss process of pitch angle diffusion for keV electrons in the inner Earth's magnetosphere. The modeling results are presented for one example storm event on February 28 - March 2, 2013 (Section 2). We take into account the electron losses by incorporating the electron lifetimes into Inner Magnetosphere Particle Transport and Acceleration Model (IMPTAM) [*Ganushkina et al.*, 2013, 2014, 2015] which is decribed in Section 3 following several models for them. We start with the case with no losses (Section 4) and, then, introduce first strong diffusion and add weak diffusion following *Chen et al*. [2005] model (Section 5). Section 6 presents the results of incorporating the electron lifetimes due to interactions with chorus waves given by *Orlova and Shprits* [2014] and hiss waves given by *Orlova et al.* [2014, 2016] obtained from the VERB code developed by *Ni et al.* [2008] and *Shprits and Ni* [2009]. The data-model comparison are made for observations at geostationary orbit by AMC12 satellite measuring electron fluxes with energies from 5 to 50 keV and inside geostationary orbit by Van Allen Probes instruments covering the energy range from 1 to 200 keV. In Section 7 we summarize the obtained results.

2 February 28 - March 2, 2013 Storm: Event Overview

For modeling, we selected the very typical storm which occurred on February 28 - March 2, 2013. Figure 1 shows the (a) IMF B_z variations, (b) solar wind velocity V_{sw}, and (c) solar wind dynamic pressure P_{sw}, observed at ACE spacecraft, (d) AE index and (e) Dst-index as SYM-H component. We used the openly available ACE data at NOAA SWPC (http://services.swpc.noaa.gov/text/) together with data from OMNIWeb (http://omniweb.gsfc.nasa.gov/) and the geomagnetic indices from the World Data Center for Geomagnetism, Kyoto (http://wdc.kugi.kyoto-u.ac.jp/wdc/Sec3.html). The storm was a CIR-driven storm with Dst index drop to about 80 nT at abut 1000 UT on March 1st. IMF B_z oscillated a lot and dropped to -15 nT at about 0830 UT on March 1st. Solar wind velocity increased from 350 to 650 km/s, solar wind dynamic pressure peaked at 8 nPa at about 1100 UT on March 1st. AE index showed increased substorm activity reaching of 800- 1400 nT in peaks. Kp index (not shown) was 1-2 during February 28th but quickly increased to 5 in the beginning of March 1st and stayed at 4 from 12 UT until 03 UT on March 2nd. During March 2nd, it was at the level of 3.

Data on low energy electron fluxes from several satellites in the inner magnetosphere were available for this storm period. It includes AMC 12, GOES 13 and GOES 15, LANL and Van Allen Probes satellites. AMC 12 geostationary satellite which was at 322.5 Deg E has a CEASE-II (Compact Environmental Anomaly Sensor) instrument [*Dichter et al.*, 1998], which contains an Electrostatic Analyzer (ESA) and is a suite of various sensors intended to measure the in-situ space environment at the host spacecraft. The instrument contains a Lightly Shielded Dosimeter, a Heavily Shielded Dosimeter, a Particle Telescope (measuring high energy electrons and protons) and an Electrostatic Analyzer for measuring low energy electron fluxes in 10 channels, covering the range 5 - 50 keV. On GOES-13 and GOES-15 satellites which are located at geostationary orbit at longitudes of 75 degrees and 135 degrees West, respectively, the MAGED (MAGnetospheric Electron Detector) instrument is a set of nine collimated solid state detectors [*Hanser*, 2011; *Rodriguez*, 2014]. The detectors operate in five energy channels of 30–50 keV, 50–100 keV, 100–200 keV, 200–350 keV, and 350–600 keV for electrons. The nine detectors, or telescopes, each with a full detection cone angle of 30 degrees, form two crossing fans with the central telescope 1 pointing directly away from the Earth. Data from six geosynchronous LANL spacecraft (1991-080, 1994-084, LANL-01A, LANL-02A, LANL-04A, LANL-97A) were available from Magnetospheric Plasma Analyzer (MPA) [*Bame et al.*, 1993]. MPA instruments are electrostatic analyzers that measure the three-dimensional energy-per-charge distributions of both ions and electron between 1 eV/q and 40 keV/q. The Van Allen Probes mission [*Mauk et al.*, 2013] consists of two spacecraft in near-equatorial elliptical orbits around Earth, traversing the inner magnetosphere at distances from 1.1 R_E to 5.8 R_E at a 9-hour period. The two satellites have slightly different orbits, with one lapping the other every 2.5 months. The HOPE (Helium Oxygen Proton Electron) instrument [*Funsten et al*., 2013], part of the Thermal plasma (ECT) suite [*Spence et al.*, 2013], measures the pitch angle distribution of electrons over the energy range from 30 eV up to 45 keV. The Magnetic Electron Ion Spectrometer (MagEIS) instrument [*Blake et al*., 2013] uses magnetic focusing and pulse height analysis to provide the cleanest possible energetic electron measurements over the critical energy range of 30 keV to 4 MeV.

We will primarily use the electron fluxes with energies from 1 to 150 keV for our analysis. These energies are most important for surface charging. Measurements onboard all available satellites overlap in this energy range which makes it very useful to comparison. Although we made the comparison with all available data, here we present the results for AMC 12 measurements at geostationary orbit and for Van Allen Probes inside geostationary orbit to keep the number of figures reasonable.

3 Modeling approach: Inner Magnetosphere Particle Transport and Acceleration Model

The IMPTAM [*Ganushkina et al.*, 2013, 2014, 2015] traces distributions of electrons in the drift approximation with arbitrary pitch angles from the plasma sheet to the inner L-shell regions with energies reaching up to hundreds of keVs in time-dependent magnetic and electric fields. We trace a distribution of particles in the drift approximation, and we take into account the $\mathbf{E} \times \mathbf{B}$ drift, and magnetic drifts with bounce-average drift velocities [*Roederer*, 1970]. Relativistic effects for electrons are taken into account in the drift velocities.

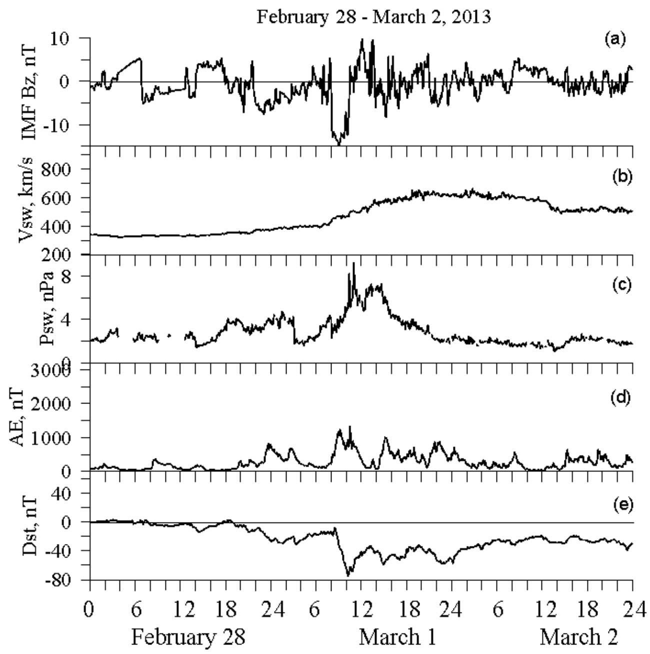

226 **Figure 1.** February 28 - March 2, 2013 Storm Event Overview: (a) IMF B_z variations, (b) solar wind velocity V_{sw}, and (c) solar wind dynamic pressure P_{sw}, measured by ACE spacecraft, (d) AE and (e) Dst-index as SYM-H component provided by the Kyoto World Data Center for Geomagnetism.

To follow the evolution of the particle distribution function f and particle fluxes in the inner magnetosphere dependent on the position R, time t, energy E_{kin}, and pitch angle α, it is necessary to specify: (1) particle distribution at initial time at the model boundary; (2) magnetic and electric fields everywhere dependent on time; (3) drift velocities; (3) all sources and losses of particles. The changes in the distribution function $f(R, \phi, t, E_{kin}, \alpha)$, where R and ϕ are the radial and azimuthal coordinates in the equatorial plane, respectively, are obtained by solving the equation $\frac{df}{dt} = \frac{\partial f}{\partial \phi} \cdot V_\phi + \frac{\partial f}{\partial R} \cdot V_R + sources - losses$, where V_ϕ and V_R are the azimuthal and radial components of the bounce-average drift velocity. The model boundary can be set in the plasma sheet at distances, depending on the scientific questions we are trying to answer, from 6.6 R_E to 10 R_E. Liouville's theorem is used to gain information of the entire distribution function by mapping the boundary conditions throughout the simulation domain, including loss process attenuation, through the time-varying magnetic and electric fields.

For the obtained distribution we apply radial and pitch angle diffusion which play significant roles in electron energization and loss. We solve the Fokker-Planck Equation for radial diffusion [*Schulz and Lanzerotti*, 1974] for the obtained distribution function. The modified Fokker-Planck Equation which also takes into account the pitch angle diffusion can be written as:

$$\frac{df}{dt} = L^2 \frac{\partial}{\partial L} |_{\mu,J} \frac{1}{L^2} D_{LL} \frac{\partial f}{\partial L} |_{\mu,J} + \frac{1}{T(\alpha_0) sin(2\alpha_0)} \frac{\partial}{\partial \alpha_0} |_{p,L} T(\alpha_0) sin(2\alpha_0) D_{\alpha\alpha} \frac{\partial f}{\partial \alpha_0} |_{p,L}, \quad (1)$$

where L is the McIlwain parameter, μ, J are the first and second adiabatic invariants, respectively, D_{LL} is the radial diffusion coefficient, α_0 is the equatorial pitch angle, p is the relativistic momentum, $D_{\alpha\alpha}$ are bounce and drift averaged diffusion coefficients, and $T(\alpha_0)$ is a function corresponding to the bounce frequency and is given by *Schulz and Lanzerotti* [1974]. Energy diffusion can be neglected for lower energy electrons and in the regions where the ratio of plasma to gyro-frequency is relatively high.

Kp-dependent radial diffusion coefficients D_{LL} for the magnetic field fluctuations are computed as $D_{LL} = 10^{0.056Kp-9.325} L^{10}$ following *Brautigam and Albert* [2000]. Since diffusion by the magnetic field fluctuations at $L > 3$ dominates diffusion produced by electrostatic field fluctuations [*Shprits and Thorne*, 2004], we ignore the electrostatic component of the radial diffusion coefficient.

The pitch angle diffusion due to wave-particle interactions can be incorporated solving Equation 1 and using $D_{\alpha\alpha}$ directly as a matrix of pitch angle diffusion coefficients dependent on L-shell, pitch-angle, and energy for various levels of geomagnetic activity. This matrix can be provided by radiation belts models, such as VERB code [*Shprits et al.*, 2008a,b]. The most important factor is the types of waves which are considered when computing this matrix. Pitch angle diffusion coefficients $D_{\alpha\alpha}$ are inversly proportional to the electron lifetimes τ. *Shprits et al.* [2006] showed that when the pitch angle diffusion coefficient (as a function of the equatorial pitch angle) does not exhibit local minima below 1/10th of the scattering rate near the edge of the loss cone, the electron lifetimes can be estimated as the inverse value of the pitch-angle diffusion coefficient near the edge of the loss cone as $\tau = \frac{1}{D_{\alpha\alpha}(\alpha_{LC})}$. In order to obtain τ, it is necessary to determine the loss cone pitch angles α_{LC} at each L-shell and find the corresponding $D_{\alpha\alpha}$ at the edge of loss cones by interpolating the available $D_{\alpha\alpha}$ at pitch angles around it. In IMPTAM we do not use the pitch angle diffusion coefficients directly, but electron lifetimes computed from them. Equation 1 will take the form:

$$\frac{df}{dt} = L^2 \frac{\partial}{\partial L} \mid_{\mu,J} \frac{1}{L^2} D_{LL} \frac{\partial f}{\partial L} \mid_{\mu,J} - \frac{f}{\tau}. \tag{2}$$

Convective outflow, Coulomb collisions and loss to the atmosphere are taken into account. We assume strong pitch angle scattering at the distances where the ratio between the radius of the field line curvature in the equatorial current sheet R_c and the effective Larmor radius ρ varies between 6 and 10 [*Sergeev and Tsyganenko*, 1982; *Buchner and Zelenyi*, 1987; *Delcourt et al.*, 1996]. Electron precipitation to the atmosphere is calculated similarly to *Jordanova et al.* [2008] with a time scale of a quarter bounce period, and the loss cone corresponds to an altitude of 200 km.

At the next time step we repeat the order of calculation: first we solve transport including radial diffusion with all other losses and then apply the pitch angle diffusion to the existing distribution function.

IMPTAM can utilize any magnetic or electric field model, including a self-consistent magnetic field. In addition to the large-scale fields, transient fields associated with the dipolarization process in the magnetotail during substorm onset were modeled (e.g., *Ganushkina et al*. [2005]) as an earthward propagating electromagnetic pulse of localized radial and longitudinal extent [*Li et al.*, 1998; *Sarris et al.*, 2002]. IMPTAM can take into account the self-consistency of the magnetic field by calculating the magnetic field produced by the model currents and feeding it back to the background magnetic field. Realistic model magnetic field such as Tsyganenko models [*Tsyganenko*, 2013] contain the prescribed ring and near-Earth tail currents. If they are used together with calculations of the induced magnetic field to trace particles in them, the obtained results will be incorrect. To be accurate, it is necessary to remove the model ring and near-Earth tail currents from the background magnetic field model and consider self-consistent calculations of the magnetic field. The Tsyganenko models produce a near-Earth nightside field that is relatively close to the field distortions from self-consistent magnetic field calculations. Since we study the electrons, their contribution to the ring current is no more than 10%, so their contribution to the distortion of the background magnetic field is small. Taking into account the electric field in a self-consistent way is of high importance when modeling the inner magnetosphere particles [*Fok et al.*, 2003; *Liemohn and Brand*, 2005]. In our study we focus on low-energy electrons which do not contribute significantly to the total pressure as compared to ions, so therefore we consider this influence to be small beyond that already included in the chosen field models and we neglect it in this study.

IMPTAM is driven by various solar wind, IMF and geomagnetic indices which are used as inputs for the different components of IMPTAM. As was shown in our previous validation studies [*Ganushkina et al.*, 2015], the best models for magnetic and electric fields used in IMPTAM which give close comparison to the observations are the Tsyganenko T96 magnetic field model [*Tsyganenko*, 1995] which uses the Dst index, P_{SW}, and IMF B_Y and B_Z as input parameters and the electric field as the *Boyle et al.* [1997] ionospheric potential mapped to the magnetosphere driven by the V_{SW}, the IMF strength B_{IMF} andB_Y and B_Z (via IMF clock angle θ_{IMF}).

We set the model boundary at 10 R_E and use the kappa electron distribution function. We set k=1.5. Although it was found that the typical energy spectra fits best by a kappa distribution with spectral slopes in the range k = 4-8 [*Vasyliunas*, 1968; *Christston et al.*, 1989, 1991], our previous results (presented as part of the review paper by *Horne et al.* [2013]) indicated that decreasing the k parameter from 5 to 1.5 gave the best agreement between the modeled and the observed electron fluxes with 50-150 keV energies at geostationary orbit onboard the LANL satellites. Other k values lower than in earlier studies were recently obtained on Cluster (k = 2.89) [*Walsh et al.*, 2013] and THEMIS (k = 2.5-3) [*Gabrielse et al.*, 2014]. In our model, we assume that the distribution can be fitted by the kappa shape only in the finite range of velocities. Parameters of the kappa distribution function are the number density n and temperature T in the plasma sheet given by the *Dubyagin et al.* [2016] empirical model, constructed at distances between 6 and 11 R_E based on THEMIS data.

4 Modeling of keV electrons at geostationary orbit with IMPTAM: Absence of losses

To investigate the importance of wave-particle interactions in loss processes for keV electrons in the inner Earth's magnetosphere, we start with the modeling of February 28-March 2, 2013 storm event without taking into account any of them. We do not introduce any lifetimes for electrons due to pitch angle diffusion. Figure 2 presents the electron fluxes at geostationary orbit observed by the CEASE II ESA instrument onboard the AMC 12 satellite for (a) 50-15 keV and (b) 15-5 keV (thick black lines) and modeled with IMPTAM for 39.7-50.7 keV (thin black lines), 31.1-39.7 keV (blue lines), 24.3-31.1 keV (green lines), 19.1-24.3 keV (red lines), 15.0-19.1 keV (pink lines), 11.8-15 keV (orange lines), 9.27-11.8 keV (magenta lines), 7.29-9.27 keV (light pink lines), 5.74-7.29 keV (light blue lines), and 4.81-5.74 keV (dark green lines) for February 28-March 2, 2013 storm. The satellite's midnight (0230 UT) and noon (1430 UT) are marked with blue and yellow vertical lines, respectively. The data are in the format of time-averaged differential fluxes $(1/(cm^2 \cdot s \cdot sr \cdot eV))$. The output from the model is integral flux $(1/(cm^2 \cdot s))$ produced by all electrons coming from all directions with energies in the ten given energy ranges. In order to be able to compare the observed and modeled fluxes more properly, we need to introduce the width of the energy channel and the solid angle 4π. So, the model electron fluxes are in model flux/($4\pi\Delta$ E).

All the variations which can be seen in the modeled low energy electron fluxes are caused by the variations in model parameters which are the solar wind and IMF parameters and Dst index included in background magnetic and electric field models and boundary conditions. As can be noted, in average, the modeled fluxes are of $10^4 1/(cm^2 \cdot s \cdot sr \cdot eV)$. No pronounced variations which are present in the observed fluxes can be seen in the modeled fluxes.

5 Modeling of keV electrons at geostationary orbit with IMPTAM: Electron lifetimes following *Chen et al*. [2005]

To start introducing electron losses due to pitch angle scattering, we consider the study by *Chen et al*. [2005] where two different models were presented. The pitch angle

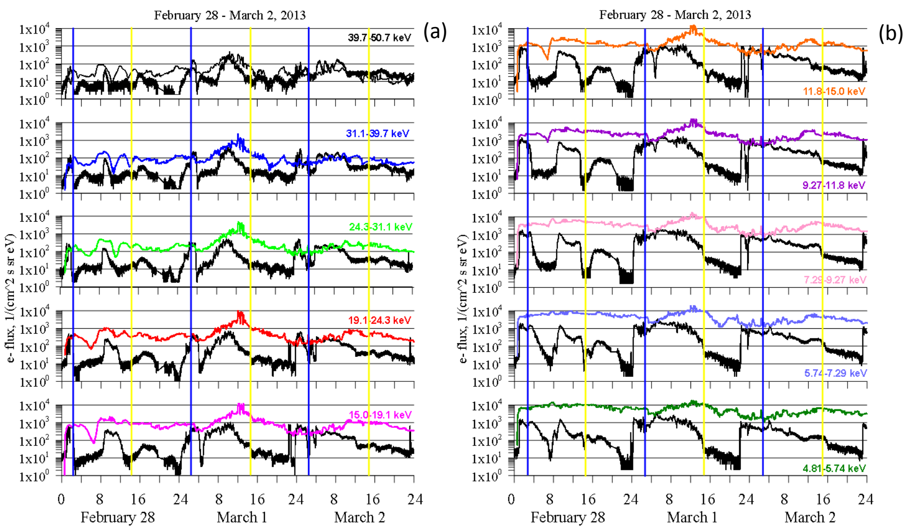

359 **Figure 2.** Electron fluxes at geostationary orbit observed by the CEASE II ESA instrument onboard the
360 AMC 12 satellite for (a) 50-15 keV and (b) 15-5 keV (thick black lines) and modeled with IMPTAM (color
361 lines) for February 28-March 2, 2013 storm. During these days, the satellite was at midnight at 0230 UT (blue
362 vertical line) and at noon at 1430 UT (yellow vertical lines). No electron losses are considered.

diffusion was represented as a combination of two regimes, first corresponds to strong pitch-angle diffusion everywhere [*Chen and Schulz*, 2001b] and second is for weak pitch angle diffusion [*Chen and Schulz*, 2001a]. The term "less than everywhere strong" scattering was used by *Chen and Schulz* [2001a] to define the diffusion which was not strong and when the electron distribution was not necessarily isotropic but we will use the term "weak" diffusion [*Kennel*, 1969; *Schulz*, 1974]. The lifetime τ_{sd} for strong pitch-angle diffusion is given as

$$\tau_{sd} = (\frac{\gamma m_0}{p})[\frac{2\Psi B_h}{1-\eta}], \qquad (3)$$

where p is the particle momentum, γ is the ratio of relativistic mass to rest mass, B_h is the magnetic field at either foot point of the field line, Ψ is the magnetic flux tube volume, $\eta = 0.25$ is the backscatter coefficient (25% of electrons that will mirror at or below 0.02 R_E are scattered back to the flux tube instead of precipitating into the atmosphere). The strong-diffusion lifetime τ_{sd} increases monotonically with radial distance. For example, the lifetime of 4 keV electrons at 6 R_E is about 20 min.

Strong pitch-angle diffusion is an ideal case. *Chen and Schulz* [2001b] stressed that there is a need for a model in which the pitch-angle diffusion is not strong everywhere (the term "less than everywhere strong" appeared because of that). The scattering rate λ_0 is approximated by

$$\lambda_0(E,R) = min[0.08(E,MeV)^{-1.32}, 0.4 \cdot 10^{2R-6+0.4log_2(E))}]day^-1, \qquad (4)$$

where energy E is measured in units of MeV. Lifetimes due to wave-particle interactions are significantly shorter than those due to Coulomb scattering at distances beyond 3.5 R_E for electrons with energies of 10-20 keV. For example, a 10-keV electron at 5 R_E has a Coulomb lifetime of 100 days, but the lifetime due to wave-particle interactions is only 2.7 hours. The MLT-dependence of the scattering rate is modeled as

$$\lambda(E,R,\phi) = [1 + a_1^* sin(\phi+\phi_0) + a_2^* cos2(\phi+\phi_0)]\lambda_0(E,R), \qquad (5)$$

where θ is the MLT coordinate, the coefficients a_1^*, a_2^*, and ϕ_0 are the adjustable parameters set as $a_1^* = 1.2$, $a_2^* = -0.25 \cdot a_1^*$, and $\phi_0 = \pi/6$. This produces less scattering in the evening and more scattering in the morning.

The corresponding electron lifetime due to weak diffusion is inversely proportional to the scattering rate, $\tau_{wd} = 1/\lambda(E,R,\phi)$. At distances < 4 R_E, the lifetimes correspond approximately to the limit of weak pitch-angle diffusion. At distances > 4 R_E, however, the lifetimes are close to the strong-diffusion lifetimes.

Figure 3 presents, in a similar format as Figure 2, the electron fluxes at geostationary orbit observed by the CEASE II ESA instrument onboard the AMC 12 satellite and modeled with IMPTAM for February 28-March 2, 2013 storm with electron losses by *Chen et al*. [2005] electron lifetimes for strong diffusion only. Flux drops to almost zero values can be seen when satellite moves to the dayside and further to the duskside. At the same time, on the nightside and at dawn, the modeled fluxes are rather to close to the observed ones, especially for electrons energies below 15 keV. Electron fluxes observed at Van Allen Probe A (a) and B (c) by HOPE and MagEIS instruments for energies from 1 to 200 keV and modeled with IMPTAM (b, d) for February 28-March 2, 2013 storm are shown in Figure 4. Figure 4 demonstrates how the inclusion of the strong diffsuion only results in rather low fluxes along Van Allen Probes A and B orbits inside geostationary distances.

Figure 5 presents, in a similar format as Figure 2, the electron fluxes at geostationary orbit observed by the CEASE II ESA instrument onboard the AMC 12 satellite and modeled with IMPTAM for February 28-March 2, 2013 storm with electron losses by *Chen et al*. [2005] electron lifetimes for strong and weak diffusion. We can clearly see that the losses are responsible for the daily decrease of the electron fluxes when satellite moves from midnight to towards dawn-noon-dusk. The agreement between the observed and modeled fluxes is quite reasonable, although the modeled fluxes are higher than the observed ones. The fluxes with electron energies from 15 to 50 keV are better modeled. Figure 6 shows the observed (a, c) and modeled (b, d) electron fluxes at Van Allen Probe A and B orbits with strong and weak diffusion taken into account. Applying the weak diffusion in addition to the strong diffusion leads to a very reasonable magnitudes of modeled fluxes and rather close to the observed evolution during the storm. Weak diffusion plays the most important role at distances inside geostationary orbit.

6 Modeling of losses of keV electrons due to wave-particle interactions with the VERB code

The quasi-linear diffusion coefficient is a powerful tool to quantify the effect of cyclotron resonance on radiation belt electrons. The Full Diffusion Code, developed by [Ni et al., 2008] and [Shprits and Ni, 2009], is capable of obtaining accurate diffusion coef-

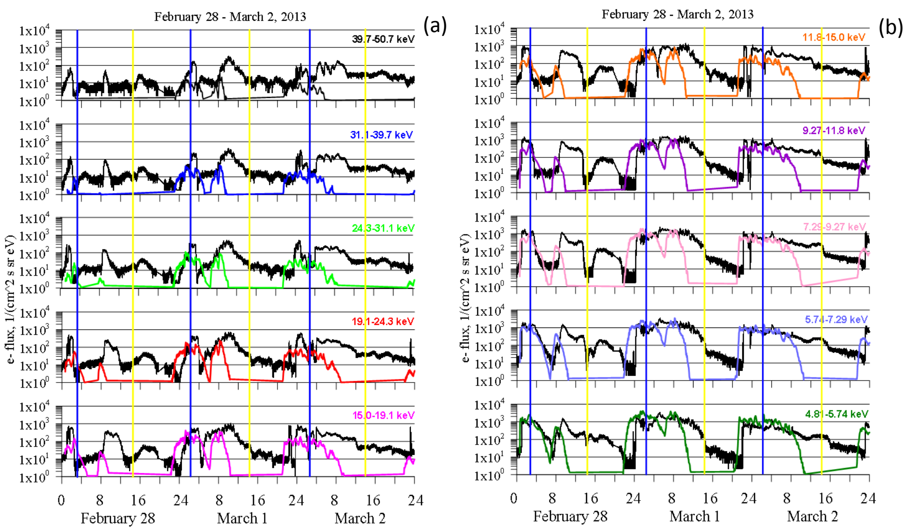

408 **Figure 3.** Electron fluxes at geostationary orbit observed by the CEASE II ESA instrument onboard the AMC 12 satellite for (a) 50-15 keV and (b) 15-5 keV (thick black lines) and modeled with IMPTAM (color lines) for February 28-March 2, 2013 storm. During these days, the satellite was at midnight at 0230 UT (blue vertical line) and at noon at 1430 UT (yellow vertical lines). Electron losses are represented following *Chen et al*. [2005] electron lifetimes for strong diffusion only.

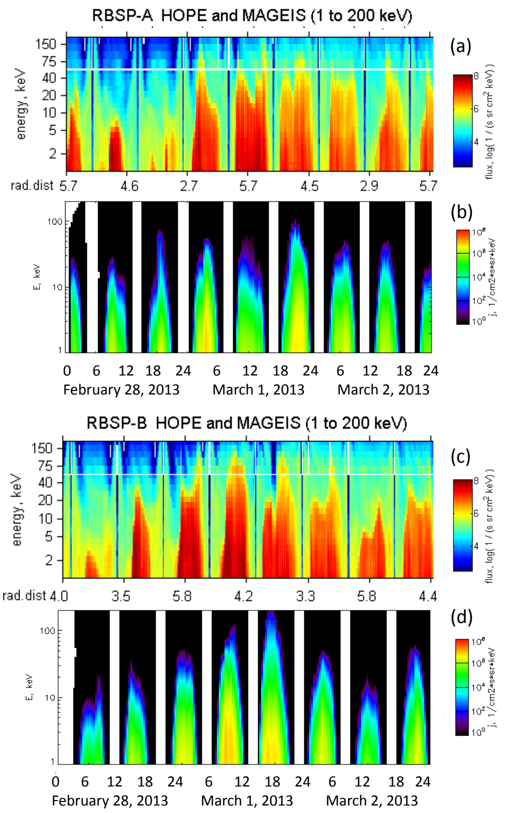

413 **Figure 4.** Electron fluxes observed at Van Allen Probe A (a) and B (c) by HOPE and MagEIS instruments
414 for energies from 1 to 200 keV and modeled with IMPTAM (b, d) for February 28-March 2, 2013 storm.
415 Electron losses are represented following *Chen et al*. [2005] electron lifetimes for strong diffusion only.

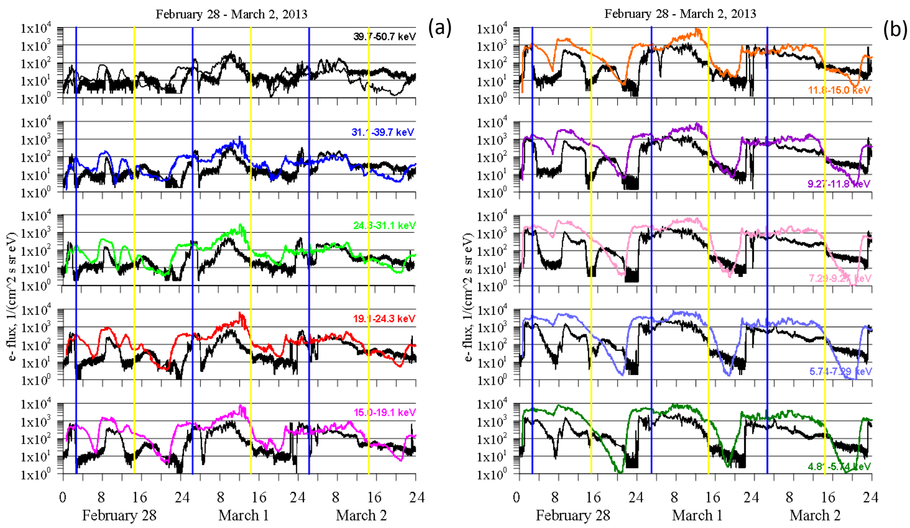

Figure 5. Electron fluxes at geostationary orbit observed by the CEASE II ESA instrument onboard the AMC 12 satellite for (a) 50-15 keV and (b) 15-5 keV (thick black lines) and modeled with IMPTAM (color lines) for February 28-March 2, 2013 storm. During these days, the satellite was at midnight at 0230 UT (blue vertical line) and at noon at 1430 UT (yellow vertical lines). Electron losses are represented following *Chen et al*. [2005] electron lifetimes for strong and weak diffusion.

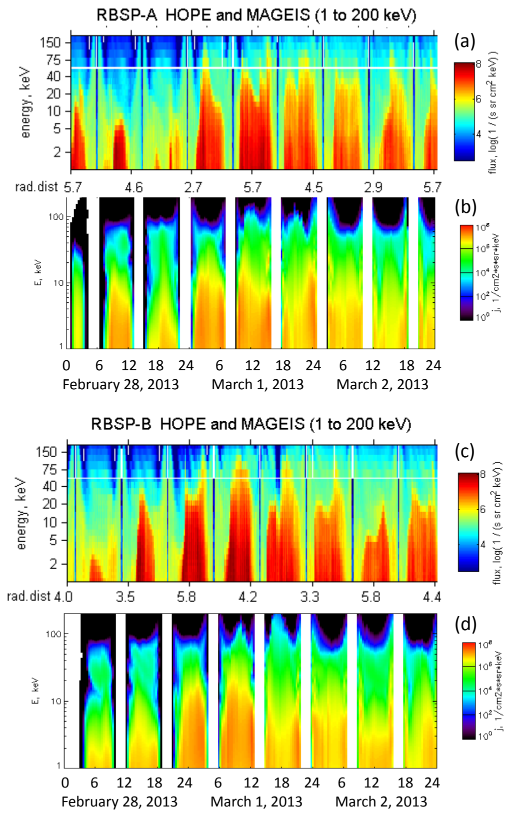

434 **Figure 6.** Electron fluxes observed at Van Allen Probe A (a) and B (c) by HOPE and MagEIS instruments
435 for energies from 1 to 200 keV and modeled with IMPTAM (b, d) for February 28-March 2, 2013 storm.
436 Electron losses are represented following *Chen et al*. [2005] electron lifetimes for strong and weak diffusion.

ficients for different waves modes, e.g. chorus, plasmaspheric hiss, Electromagnetic Ion Cyclotron (EMIC) and magnetosonic waves [Orlova and Shprits, 2010; Orlova et al. 2012; Shprits et al. 2013.]. FDC uses a parallel architecture and calculations are performed on NCAR's YellowStone supercomputer and UCLA's Hoffman2 Cluster.

There are two ways to estimate the electron's lifetime based on diffusion coefficients. One is the inverse of pitch angle diffusion coefficients at loss cone [*Shprits et al.*, 2006], which can be applied when the pitch angle diffusion coefficients do not drop below 1/10 of the value near the edge of the loss cone, α_{LC}, for up to a 30 degrees wide range of pitch angle. One is estimated by the integral of 1/(Dtanα) [*Albert and Shprits*, 2009], which is simpler and physically more transparent than the full calculation, and allows convenient estimates of changing various wave parameters.

If the scattering rates as functions of pitch angle are relatively monotonic or, at least, do not show significant minima of one order of magnitude or more, the times of losses can be estimated by taking an inverse of the pitch angle scattering rates near the edge of the loss cone [*Lichtenberg and Lieberman*, 1983; *Shprits et al.*, 2006]. As was noted by *Orlova et al.* [2016], if the pitch angle diffusion coefficients have a deep local minimum for a wide range of pitch angles, they can create bottleneck and slow down the overall rate of pitch angle scattering. *Orlova et al.* [2016] used the expression given by *Albert and Shprits* [2009] that utilizes pitch angle diffusion rates at all values of equatorial pitch angle to calculate electron lifetime, τ:

$$\tau = \int_{\alpha_{LC}}^{\pi/2} d\alpha_{eq} (2 < D_{\alpha\alpha} > tan(\alpha_{eq}))^{-1}, \tag{6}$$

where α_{eq} is the equatorial pitch angle and α_{LC} is the equatorial loss cone angle. As was described above, $D_{\alpha\alpha}$ is the bounce-averaged pitch angle diffusion coefficient computed in the dipole field using an approach of *Glauert and Horne* [2005] and *Albert* [2005].

6.1 Electron lifetimes due to interactions with chorus waves

VERB code and Full Diffusion Code inside it computes the bounce-averaged pitch angle diffusion coefficients and, as an output, it provides the multi-dimentional matrix with dependencies on energy, pitch angle, MLT, and Kp. The matrix of electron lifetimes is computed from the matrix of diffusion coefficients. *Orlova and Shprits* [2014] introduced the parameterization for electron lifetimes due to interactions with chorus waves, and this parameterization is now used in IMPTAM instead of the matrix of electron lifetimes.

The initial parameterizations for electron lifetimes were presented in *Orlova and Shprits* [2014]. The parameterization of electron lifetimes τ_{chorus} has the following form:

$$
\begin{aligned}
log(\tau_{chorus}) = a_1 + a_2 R + a_3 R(Kp+1) + a_4 R(Kp+1)E + a_5 R(Kp+1)E^2 + a_6 R(Kp+1)^2 + \\
+a_7 R(Kp+1)^2 E + a_8 R(Kp+1)^3 + a_9 RE + a_{10} RE^2 + a_{11} RE^3 + a_{12} R^2 + \\
+a_{13} R^2(Kp+1) + a_{14} R^2(Kp+1)E + a_{15} R^2(Kp+1)^2 + a_{16} R^2 E + \\
+a_{17} R^2 E^2 + a_{18} R^3 + a_{19} R^3(Kp+1) + a_{20} R^3 E + a_{21}(Kp+1) + \\
+a_{22}(Kp+1)E + a_{23}(Kp+1)E^2 + a_{24}(Kp+1)E^3 + a_{25}(Kp+1)^2 + \\
+a_{26}(Kp+1)^2 E + a_{27}(Kp+1)^2 E^2 + a_{28}(Kp+1)^3 + a_{29}(Kp+1)^3 E + \\
+a_{30} E + a_{31} E^2 + a_{32} E^3 + a_{33} E^4, \quad (7)
\end{aligned}
$$

where E is in MeV units, and τ_{chorus} is in days. It is valid at distances from 3 to 8 R_E, for Kp from 0 to 6, and for electron energies from 1 keV to 2 MeV.

The coefficients $a_1 - a_{33}$ were computed for four MLT sectors: night ($21 < MLT < 3$), dawn ($3 < MLT < 9$), prenoon ($9 < MLT < 12$), and postnoon ($12 < MLT < 15$). For nightside, there are 5 subsets of coefficients: (1) for E ≤ 10 keV and for all values of Kp; (2) for 10 keV $< E <$ 0.5 MeV for Kp ≤ 3; (3) for 10 keV $< E <$ 0.5 MeV for Kp > 3; (4) for E ≥ 0.5 MeV for Kp ≤ 3; and (5) for E ≥ 0.5 MeV for Kp > 3. For dawnside, 3 subsets of coefficients correspond to 3 energy intervals, such as, (1) E < 7 keV; (2) 7 keV < E < 0.1 MeV; (3) E > 0.1 MeV, and for all values of Kp. Similarly, the coefficients for prenoon and postnoon sectors are for all values of Kp and for 3 energy intervals, namely, (1) E < 7 keV; (2) 7 keV < E < 90 keV; (3) E > 90 keV. In total, there are 14 sets of coefficients used for different combinations of MLT, energy and Kp. We used the updated coefficients provided by K. Orlova. Figure 7 shows the computed equatorial maps of electron lifetimes due to interactions with chorus waves at distances from 3 to 8 R_E based on updated parameterization by *Orlova and Shprits* [2014]. For illustration and since we consider mainly the electrons in the energy range from 1 to 150 keV, we present the lifetimes for energies of 5 keV (a, b), 10 keV (c, d), 50 keV (e, f), 100 keV (g, h), and 150 (i, j) keV for two Kp values of 1 (a, c, e, g, i) and 5 (b, d, f, h, j) representing quiet and disturbed conditions per each energy. The decrease in lifetimes of electrons can be seen for all energies with the Kp increase. The parameterization does not include the lifetimes in the 15-21 MLT sector due to the lack of measurements in that sector and absence of chorus waves there which makes impossible to construct a model there.

We incorporated the electron lifetimes due to interactions with chorus waves into the IMPTAM. For the 15-21 MLT sector we set the lifetime to be equal of 100 days, since the electrons are expected to spend quite a long time in that sector (*Yu. Shprits, private communication, 2016*).

6.2 Electron lifetimes due to interactions with hiss waves

The parameterization of electron lifetimes due to interactions with hiss waves was obtained by *Orlova et al.* [2014] for two MLT sectors separately. For the nightside sector for 21-06 MLT, the τ_{hissn} is given as:

$$\begin{aligned}
log(\tau_{hissn}) = a_1 + a_2R + a_3E + a_4Kp + a_5R^2 + a_6RE + \\
+a_7E^2 + a_8RKp + a_9RE + a_{10}Kp^2 + a_{11}R^3 + a_{12}R^2E + \\
+a_{13}RE^2 + a_{14}E^3 + a_{15}R^2Kp + a_{16}REKp + \\
+a_{17}E^2Kp + a_{18}R^4 + a_{19}R^3E + a_{20}R^2E^2 + a_{21}RE^3 + \\
+a_{22}E^4 + a_{23}R^3Kp + a_{24}R^2EKp + a_{25}RE^2Kp + \\
+a_{26}E^3Kp + a_{27}R^4E + a_{28}R^3E^2 + a_{29}R^2E^3 + \\
+a_{30}RE^4 + a_{31}E^5 + a_{32}R^3EKp + a_{33}R^2E^2Kp + a_{34}RE^3Kp + \\
+a_{35}E^4Kp + a_{36}R^3E^3 + a_{37}R^2E^4 + a_{38}RE^5 + a_{39}E^6 + \\
+a_{40}R^3E^2Kp + a_{41}R^2E^3Kp + a_{42}RE^4Kp + a_{43}E^5Kp + \\
+a_{44}R^3E^4 + a_{45}R^2E^5 + a_{46}RE^6 + a_{47}E^7 + a_{48}R^3E^3Kp + \\
+a_{49}R^2E^4Kp + a_{50}RE^5Kp + a_{51}E^6Kp + a_{52}RE^7 + a_{53}E^8 + \\
+a_{54}R^2E^5Kp + a_{55}RE^6Kp + a_{56}E^7Kp + a_{57}RE^8 + a_{58}E^9 + \\
+a_{59}RE^7Kp, \qquad (8)
\end{aligned}$$

where $E = log(E_k)$, E_k is in MeV units and from 1 keV to 10 MeV. It is valid at distances from 3 to 6 R_E and for Kp up to 6.

On the dayside for 06-21 MLT, the parameterization for τ_{hissd} has the form:

$$log(\tau_{hissd}) = g(E, R) + y(Kp), \qquad (9)$$

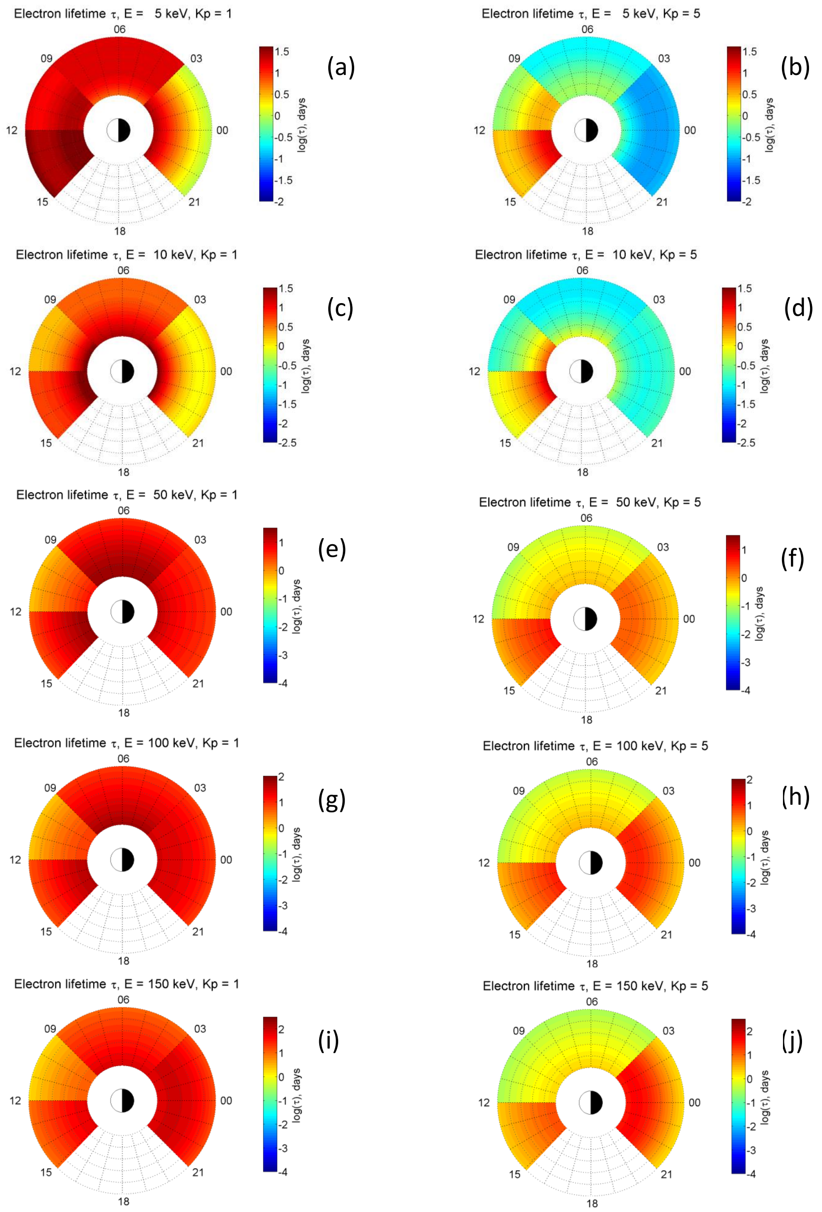

504 **Figure 7.** Equatorial maps of electron lifetimes due to interactions with chorus waves at distances from 3 to
505 8 R_E based on updated parameterization by *Orlova and Shprits* [2014].

where

$$\begin{aligned} g(E,R) = a_1 + a_2R + a_3E + a_4R^2 + a_5RE + a_6E^2 + \\ + a_7R^3 + a_8R^2E + a_9RE^2 + a_{10}E^3 + a_{11}R^4 + a_{12}R^3E + \\ + a_{13}R^2E^2 + a_{14}RE^3 + a_{15}E^4 + a_{16}R^4E + \\ + a_{17}R^3E^2 + a_{18}R^2E^3 + a_{19}RE^4 + a_{20}E^5 + a_{21}R^3E^3 + \\ + a_{22}R^2E^4 + a_{23}RE^5 + a_{24}E^6 + a_{25}R^3E^4 + \\ + a_{26}R^2E^5 + a_{27}RE^6 + a_{28}E^7 \end{aligned} \tag{10}$$

and

$$y(Kp) = 0.015465Kp^2 - o.26074Kp + 1.0077. \tag{11}$$

The obtained parameterization is only valid for $E = log(E_k) > f(L)$, where $f(L) = -0.2573R^4 + 4.2781R^3 - 25.9348R^2 + 66.8113R - 66.1182$. Figure 8 demonstrates the validity of the obtained parameterization by showing the $f(L)$ at distances from 3 to 6 R_E (upper panel) and computed energy limit (lower panel). The Equations 8 and 10 are not valid at energies below 350 keV at 3 R_E and at energies below 75 keV at 3.5 R_E with invalidity range decreasing very rapidly at larger distances.

We used the coefficients provided by K. Orlova. Figure 9 shows the computed equatorial maps of electron lifetimes due to interactions with hiss waves with the validity range taken into account at distances from 3 to 6 R_E based on the parameterization by *Orlova et al.* [2014]. We present the lifetimes for energies of 5 keV (a, b), 10 keV (c, d), 50 keV (e, f), 100 keV (g, h), and 150 (i, j) keV for two Kp values of 1 (a, c, e, g, i) and 5 (b, d, f, h, j) representing quiet and disturbed conditions per each energy. The decrease in lifetimes of electrons can be seen for all energies with the Kp increase.

Recently, new parameterization of electron lifetimes due to interactions with hiss waves were released based on the previous study by *Spasojevic et al.* [2015]. The range of distances where parameterization is valid was increased being from 1.5 to 5.5 R_E. It is applicable for Kp up to 5. The form for $\tau_{hissnew}$ is now the same for all MLTs:

$$\tau_{hissnew}(R,E,MLT,Kp) = \frac{\tau_{av}(R,E)}{g(MLT)h(Kp)}, \tag{12}$$

where $E = log(E_k)$, E_k is in MeV units and τ_{av} is the the lifetime for the averaged MLT and Kp values as a function of electron kinetic energy E_k from 1 keV up to 10 MeV and

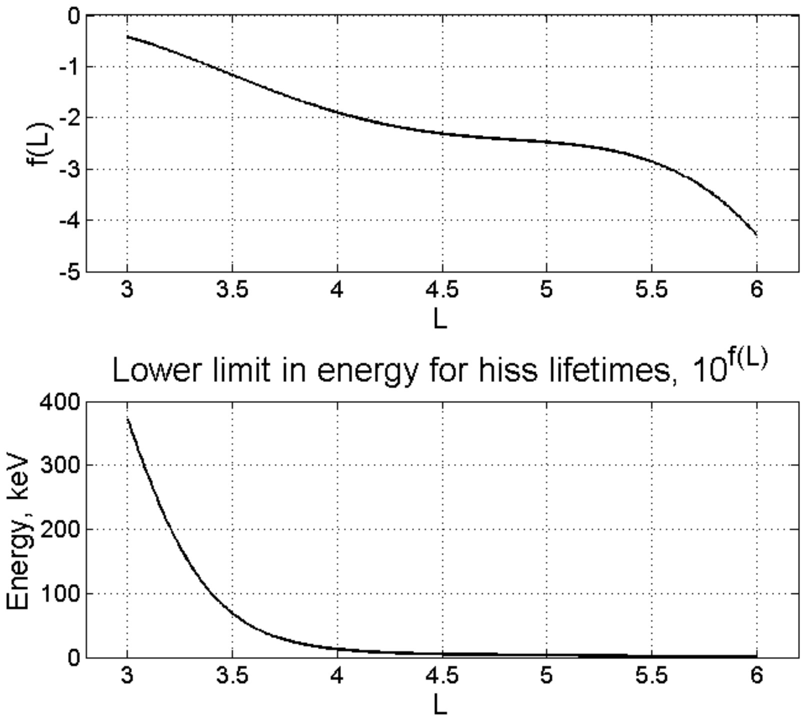

546 **Figure 8.** Validity of electron lifetimes due to interactions with hiss waves parameterization by *Orlova et*
547 *al.* [2014].

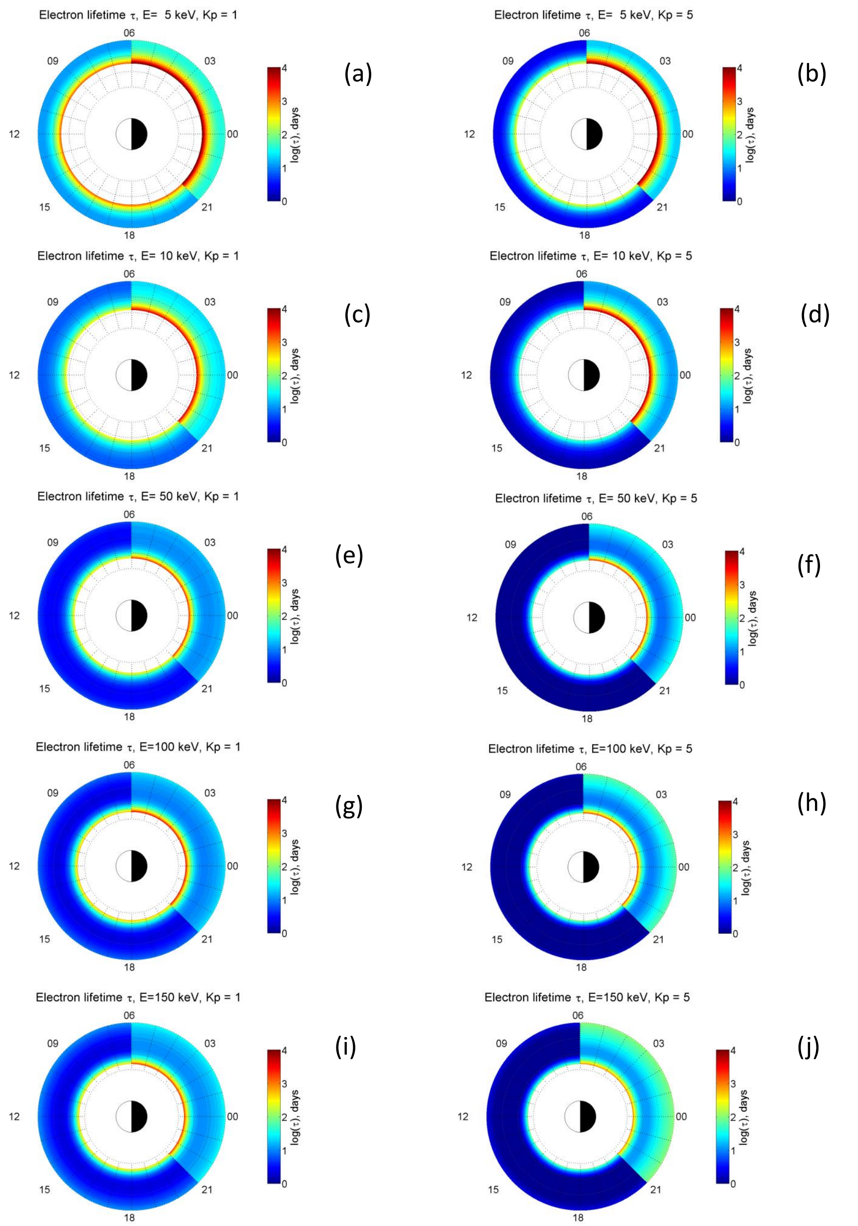

Figure 9. Equatorial maps of electron lifetimes due to interactions with hiss waves at distances from 3 to 6 R_E based on the parameterization by *Orlova et al.* [2014].

L shells from 1.5 to 5.5 which is given as

$$
\begin{aligned}
log(\tau_{av}(R,E)) = a_1 + a_2 R + a_3 E + a_4 R^2 + a_5 RE + a_6 E^2 + \\
+ a_7 R^3 + a_8 R^2 E + a_9 RE^2 + a_{10} E^3 + a_{11} R^4 + a_{12} R^3 E + \\
+ a_{13} R^2 E^2 + a_{14} RE^3 + a_{15} E^4 + a_{16} RE^4 + \\
+ a_{17} R^2 E^3 + a_{18} R^4 E + a_{19} R^5 + a_{20} E^5
\end{aligned}
\tag{13}
$$

and $g(MLT)$ and $h(Kp)$ are dimentionless scaling factors. $g(MLT) = \frac{1}{G_0} 10^{g_0(MLT)}$, $g_0(MLT) = b_2 mlt^2 + b_1 MLT + b_0$, where $G_0 = 782.3$, $b_2 =$ -0.0073, $b_1 = 0.18$, and $b_0 =$ 2.080. $h(Kp) = \frac{1}{H_0} 10^{h_0(Kp)}$, $h_0(Kp) = c_2 Kp^2 + c_1 Kp + c_0$, where $H_0 = 1315$, $c_2 =$ -0.0014, $c_1 = 0.23$, and $c_0 = 2.598$. We used the coeeficients provided in *Orlova et al.* [2016].

The obtained parameterization is only valid for $E = log(E_k) > f(L)$, where $f(L) = 0.1328R^2 - 2.1463R + 3.7857$. Figure 10 demonstrates the validity of the obtained parameterization by showing the $f(L)$ at distances from 2.5 to 5.5 R_E (upper panel) and computed energy limit (lower panel). The limits are lower than in the previous parameterization by *Orlova et al.* [2014]. The Equation 12 and 13 are not valid at energies below 200 keV at 2.5 R_E and at energies below 10 keV at 3.5 R_E with invalidity range decreasing very rapidly at larger distances.

Figure 11 shows the computed equatorial maps of electron lifetimes due to interactions with hiss waves with the validity range taken into account at distances from 1.5 to 5.5 R_E based on the parameterization by *Orlova et al.* [2016]. We present the lifetimes for energies of 5 keV (a, b), 10 keV (c, d), 50 keV (e, f), 100 keV (g, h), and 150 (i, j) keV for two Kp values of 1 (a, c, e, g, i) and 5 (b, d, f, h, j) representing quiet and disturbed conditions per each energy. The decrease in lifetimes of electrons can be seen for all energies with the Kp increase.

6.3 Combined losses due to chorus and hiss waves

We combined the represenations for both chorus and hiss waves in order to take into account their influence on the electron lifetimes. We applied the lifetimes due to chorus waves interactions at distances from 10 to 6 R_E and lifetimes due to hiss waves interactions at distances from 6 to 3 R_E for *Orlova et al.* [2014] parameterization and at distances from 5.5 to 3 R_E for *Orlova et al.* [2016] parameterization. Figure 12 shows the combined equatorial maps of electron lifetimes due to interactions with chorus and

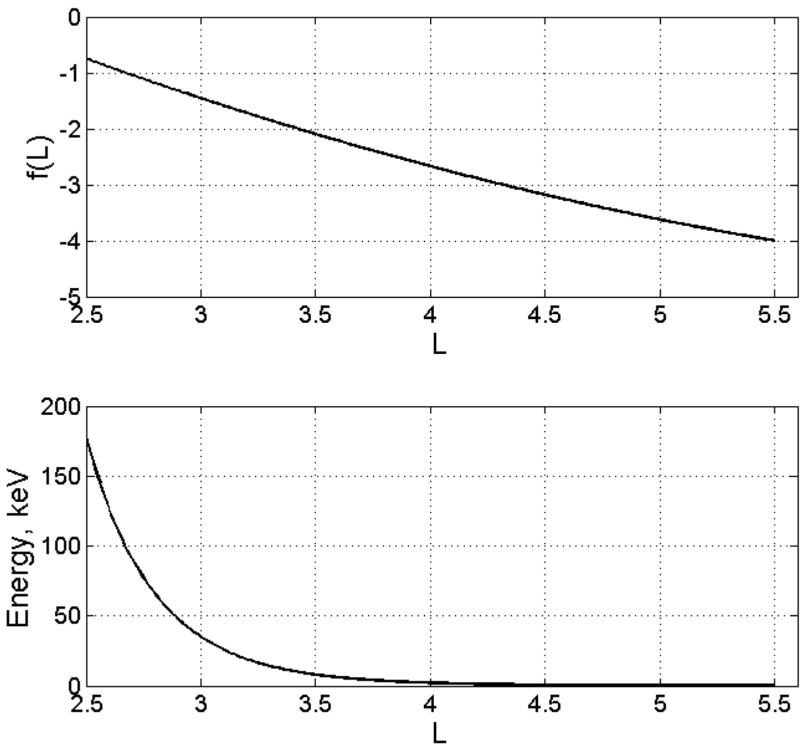

580 **Figure 10.** Validity of electron lifetimes due to interactions with hiss waves parameterization by *Orlova et*
581 *al.* [2016].

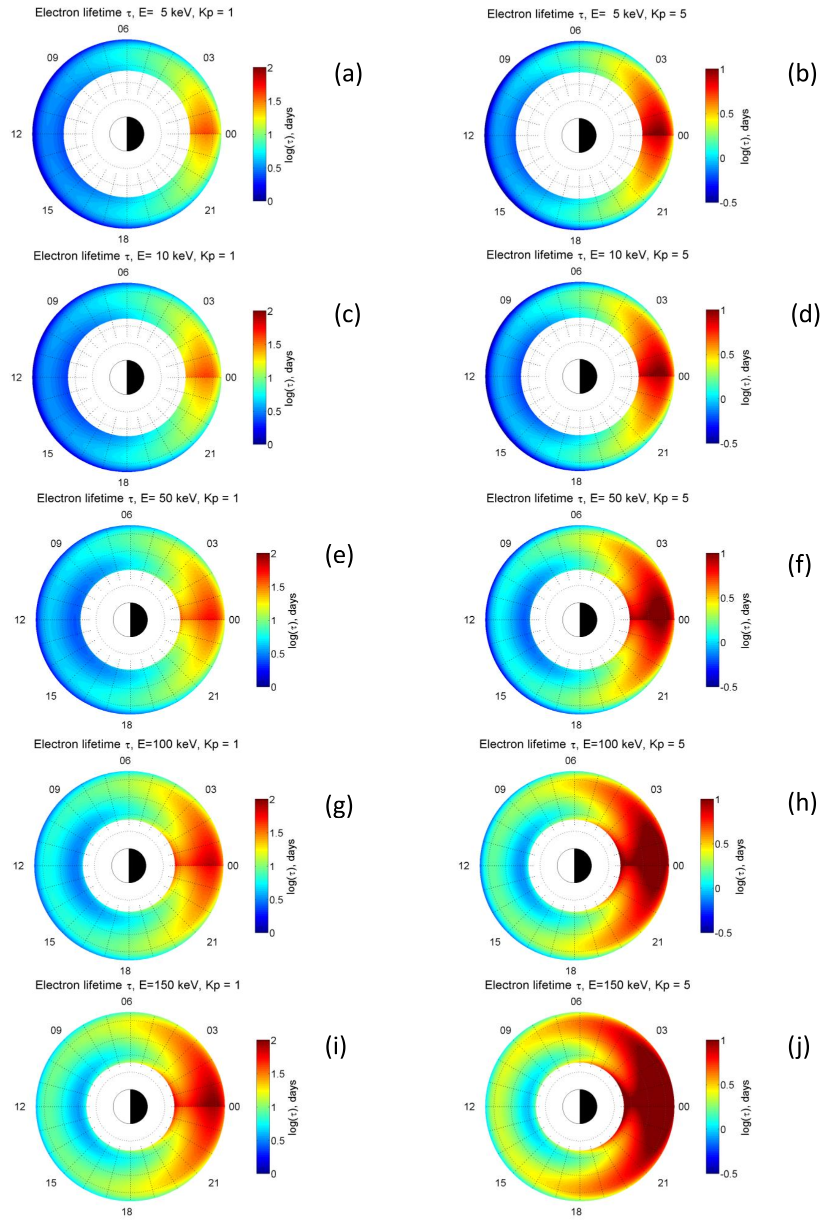

Figure 11. Equatorial maps of electron lifetimes due to interactions with hiss waves at distances from 1.5 to 5.5 R_E based on the parameterization by *Orlova et al.* [2016].

hiss waves based on the parameterizations by *Orlova and Shprits* [2014] and *Orlova et al.* [2014], respectively. We present the lifetimes for energies of 5 keV (a, b), 10 keV (c, d), 50 keV (e, f), 100 keV (g, h), and 150 (i, j) keV for two Kp values of 1 (a, c, e, g, i) and 5 (b, d, f, h, j) representing quiet and disturbed conditions per each energy.

Figure 13 presents the electron fluxes at geostationary orbit observed by the CEASE II ESA instrument onboard the AMC 12 satellite and modeled with IMPTAM for February 28-March 2, 2013 storm with electron losses due to interactions with chorus waves at distances from 10 to 6 R_E [*Orlova and Shprits*, 2014] and with hiss waves at distances from 6 to 3 R_E [*Orlova et al.*, 2014]. We can see that the observed geostationary electron fluxes are better reproduced as compared to those in Figure 5, especially during the storm maximum which occurred at around 10 UT on March 1st. It is clear that the fluxes of electrons with energies from 15 to 50 keV (Figure 13a) are better reproduced than those with lower energies between 5 and 15 keV (Figure 13b). The discrepancy between the modeled and the observed fluxes is rather pronounced (reaching even 2 orders of magnitude difference) during the first day of modeling on February 28th which was before the storm has occurred, especially for lower energies (Figure 13b). Also, at the end of the last day of the storm on March 2nd, the modeled fluxes are around one order of magnitude higher than the observed ones at noon and dusk. Since we present the modeled fluxes at geostationary orbit, the main contribution is expected to come from chorus waves in electron lifetimes (chorus waves are present at distances from 10 to 6 R_E) but hiss waves can also play their role, since the L-shell of geostationary orbit changes during the storm due to changes in the magnetic field in the surrponding region. The way how the electron lifetimes were parameterized for low energies may be the reason of the disagreement between the modeled and the observed fluxes. On the nightside, for energies less than 10 keV, coefficients in the Equation 7 are the same for all the energies and Kp values. At the same time, on February 28th the Kp was 2 but on March 1st it was 5. Even the Equation 7 contains the Kp-dependence, it is still not clear how different can be electron losses for different energies within the interval from 1 to 10 keV. For dawn, prenoon and postnoon sectors, the coefficients in the Equation 7 are the same for all Kp values and they depend on energy. The energy ranges are rather big, being, for example, from 7 keV to 90 keV at dawn. Using the same coefficients for energies of 10 and 50 keV may lead to the obtained discrepancies. Same arguments can be applied to the parameterization of electron

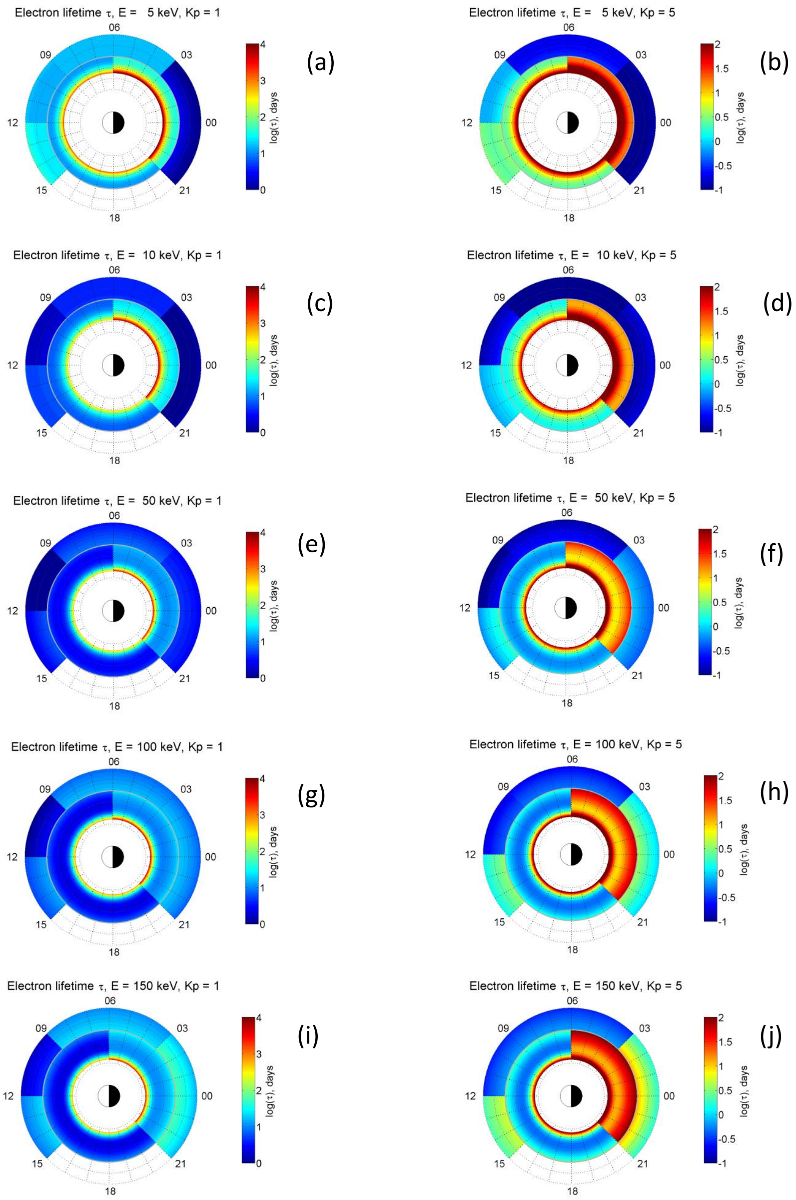

Figure 12. Equatorial maps of electron lifetimes due to interactions with chorus waves at distances from 10 to 6 R_E [*Orlova and Shprits*, 2014] and with hiss waves at distances from 6 to 3 R_E [*Orlova et al.*, 2014].

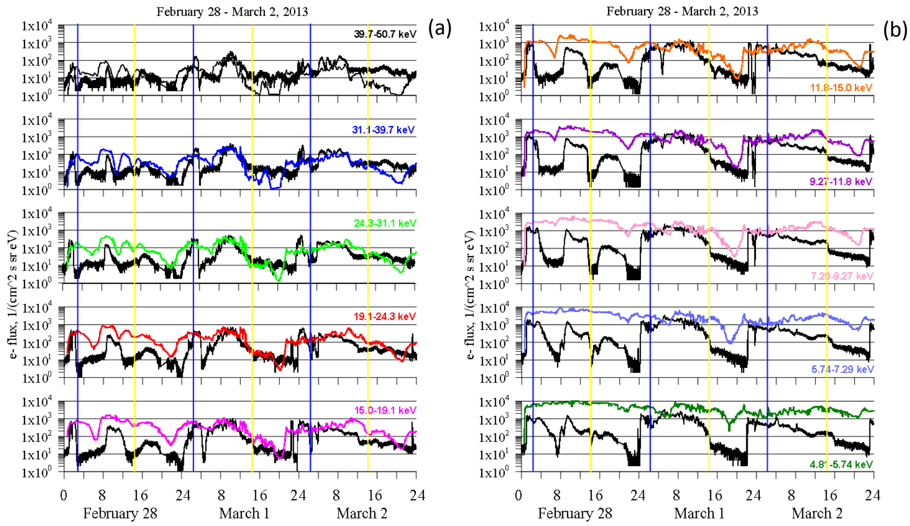

Figure 13. Electron fluxes at geostationary orbit observed by the CEASE II ESA instrument onboard the AMC 12 satellite for (a) 50-15 keV and (b) 15-5 keV (thick black lines) and modeled with IMPTAM (color lines) for February 28-March 2, 2013 storm. During these days, the satellite was at midnight at 0230 UT (blue vertical line) and at noon at 1430 UT (yellow vertical lines). Electron losses are due to interactions with chorus waves at distances from 10 to 6 R_E [*Orlova and Shprits*, 2014] and with hiss waves at distances from 6 to 3 R_E [*Orlova et al.*, 2014].

lifetimes due to hiss waves. There, only 2 sets of coefficients (dayside and nightside) are used for all energies (Equations 8 and 10).

Figure 14 shows the observed (a, c) and modeled (b, d) electron fluxes at Van Allen Probe A and B orbits. The main feature is that the modeled fluxes inside geostationary orbit are about one order of magnitude lower than the observed ones. All the arguments presented above for the results at geostationary orbit are valid here, too. Moreover, the simple combination of the electron lifetimes due to chorus and hiss waves has non-smooth transitions between them at 6 R_E where lifetime due to chorus goes into the lifetime due to hiss. Moreover, transitions between MLT-sectors inside both models are also with some jumps. This also can lead to rather complicated behavior or modeled fluxes.

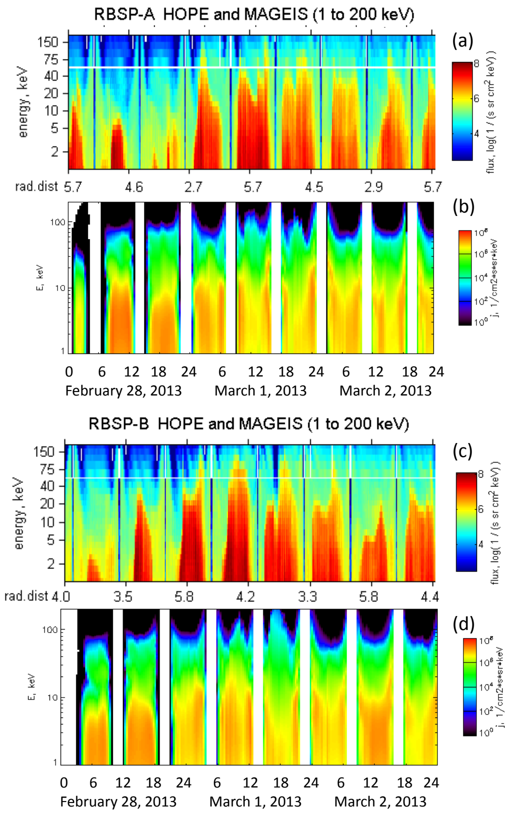

Figure 14. Electron fluxes observed at Van Allen Probe A (a) and B (c) by HOPE and MagEIS instruments for energies from 1 to 200 keV and modeled with IMPTAM (b, d) for February 28-March 2, 2013 storm. Electron losses are due to interactions with chorus waves at distances from 10 to 6 R_E [*Orlova and Shprits*, 2014] and with hiss waves at distances from 6 to 3 R_E [*Orlova et al.*, 2014].

Figure 15 shows the combined equatorial maps of electron lifetimes due to interactions with chorus and hiss waves based on the parameterizations by *Orlova and Shprits* [2014] and *Orlova et al.* [2016], respectively. We present the lifetimes for energies of 5 keV (a, b), 10 keV (c, d), 50 keV (e, f), 100 keV (g, h), and 150 (i, j) keV for two Kp values of 1 (a, c, e, g, i) and 5 (b, d, f, h, j) representing quiet and disturbed conditions per each energy.

Figure 16 presents the electron fluxes at geostationary orbit observed by the CEASE II ESA instrument onboard the AMC 12 satellite and modeled with IMPTAM for February 28-March 2, 2013 storm with electron losses due to interactions with chorus waves at distances from 10 to 5.5 R_E [*Orlova and Shprits*, 2014] and with hiss waves at distances from 5.5 to 3 R_E [*Orlova et al.*, 2016]. As it can be seen, the difference between Figure 13 and Figure 16 is not very big. The observed geostationary electron fluxes are reproduced well during the storm maximum at around 10 UT on March 1st. The fluxes of electrons with energies from 15 to 50 keV are better reproduced than those with lower energies between 5 and 15 keV but for the new hiss model, the fluxes with lower energies are closer to the observed ones (Figure 16b). Figure 17 shows the observed (a, c) and modeled (b, d) electron fluxes at Van Allen Probe A and B orbits. It is also rather similar to Figure 14 where previous representation for hiss waves was used. All the arguments presented above for the results with previous representation for hiss waves are valid here, too.

7 Discussion and Conclusions

We investigated the role of the loss process of pitch angle diffusion for keV electrons in the inner Earth's magnetosphere. We presented the modeling results for one example storm event on February 28 - March 2, 2013. The losses were taken into account by incorporating the electron lifetimes into Inner Magnetosphere Particle Transport and Acceleration Model (IMPTAM) following several models. They included (1) no losses at all, (2) losses presented as strong diffusion everywhere in the inner magnetosphere and (3) taking into account weak diffusion in addition to strong strong diffusion following *Chen et al*. [2005] model without specifying the waves responsible for pitch angle scattering, (4) losses due to interactions with specific waves, such as chorus waves (electron lifetimes given by *Orlova and Shprits* [2014]) and hiss waves (electron lifetimes given by *Orlova et al.* [2014]), and (5) losses due to interactions with chorus waves (electron lifetimes given

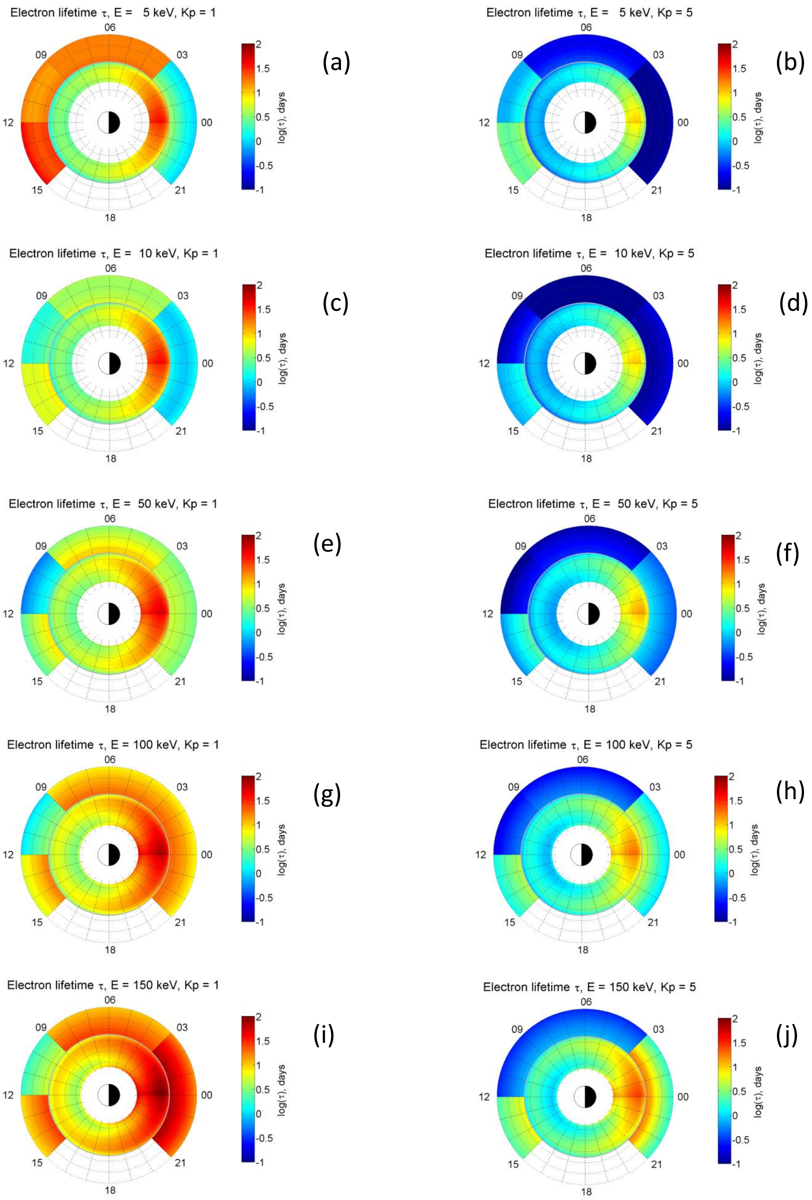

658 **Figure 15.** Equatorial maps of electron lifetimes due to interactions with chorus waves at distances from 10
659 to 6 R_E [*Orlova and Shprits*, 2014] and with hiss waves at distances from 1.5 to 5.5 R_E [*Orlova et al.*, 2016].

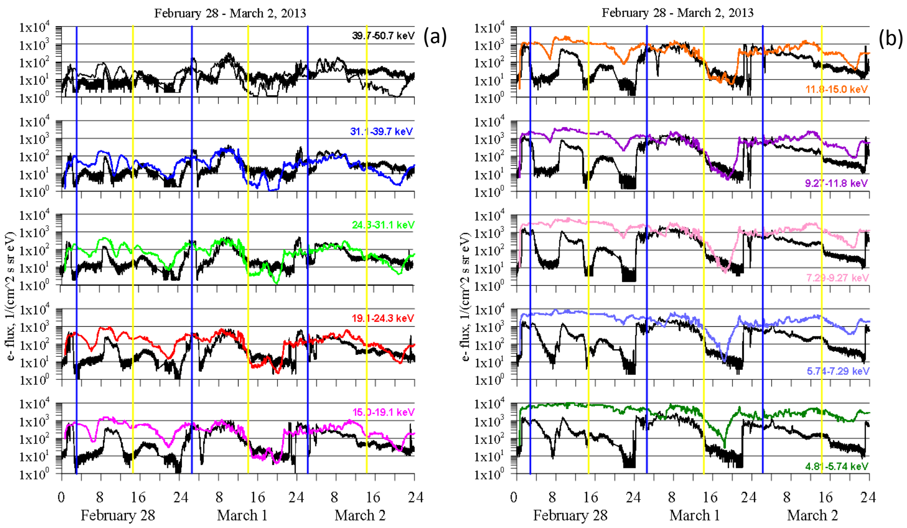

Figure 16. Electron fluxes at geostationary orbit observed by the CEASE II ESA instrument onboard the AMC 12 satellite for (a) 50-15 keV and (b) 15-5 keV (thick black lines) and modeled with IMPTAM (color lines) for February 28-March 2, 2013 storm. During these days, the satellite was at midnight at 0230 UT (blue vertical line) and at noon at 1430 UT (yellow vertical lines). Electron losses are due to interactions with chorus waves at distances from 10 to 5.5 R_E [*Orlova and Shprits*, 2014] and with hiss waves at distances from 5.5 to 3 R_E [*Orlova et al.*, 2016].

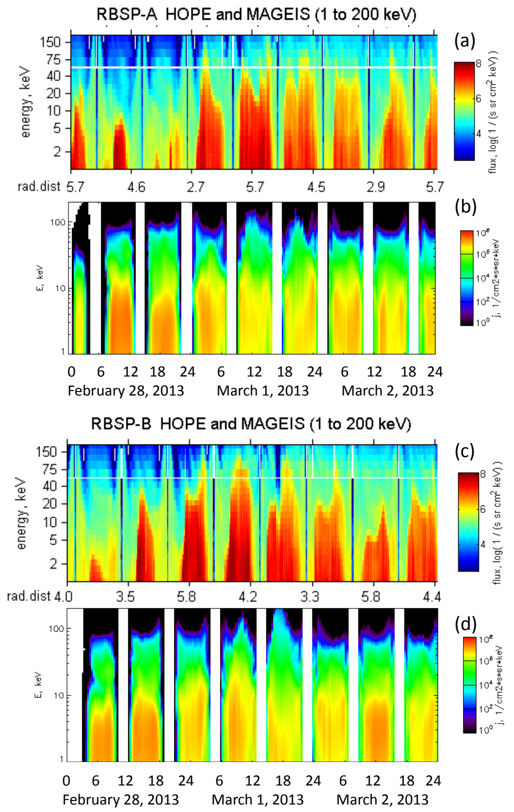

Figure 17. Electron fluxes observed at Van Allen Probe A (a) and B (c) by HOPE and MagEIS instruments for energies from 1 to 200 keV and modeled with IMPTAM (b, d) for February 28-March 2, 2013 storm. Electron losses are due to interactions with chorus waves at distances from 10 to 5.5 R_E [*Orlova and Shprits*, 2014] and with hiss waves at distances from 5.5 to 3 R_E [*Orlova et al.*, 2016].

by *Orlova and Shprits* [2014]) and hiss waves (electron lifetimes given by *Orlova et al.* [2016]). Last two models were obtained from the VERB code. We compared the modeled electron fluxes at geostationary orbit with the measurements from AMC12 satellite for energies from 5 to 50 keV and inside geostationary orbit with measurements from Van Allen Probes HOPE and MagEIS instruments covering the energy range from 1 to 200 keV.

In the absence of electron losses, all variations which can be seen in the modeled low energy electron fluxes at geostationary orbit are caused by the variations in IMPTAM's parameters which are the solar wind and IMF parameters and Dst index included in background magnetic and electric field models and boundary conditions. The modeled fluxes are of $10^4 1/(cm^2 \cdot s \cdot sr \cdot eV)$ without any pronounced variations which are present in the observed fluxes. As was demonstrated by *Ganushkina et al.* [2013], simple running of the IMPTAM with the observed parameters does not result in the model output comparable to the observed electron fluxes at geostationary orbit, if no proper loss processes are considered.

The inclusion of the strong diffusion [*Chen and Schulz*, 2001b; *Chen et al*., 2005] everywhere in the inner magnetosphere as the only process to represent the pitch angle diffusion for electrons, results in rather significant flux drops, to almost zero values, at geostationary orbit on the day- and duskside. At the same time, on the nightside and at dawn, the modeled fluxes are rather to close to the observed ones, especially for electrons energies below 15 keV. The electron fluxes are rather low inside geostationary orbit. This finding agrees well with the study by *Chen et al*. [2015] where they used the same model of *Chen and Schulz* [2001b] for strong diffusion and modeled August 10, 2000 storm event with RMC-E code [*Lemon et al.*, 2004] considering that all loss for electrons comes from the strong diffusion only. For data-model comparison, they used the 18 hours energy-time spectrogram from one LANL 1994-084 satellite. They found that on the dayside from 0900 to 1730 MLT, there is too much of flux depletion. At the same time, on the nightside the modeled electron fluxes were of the order of magnitude comparable to the observed ones. If only the strong diffusion is considered, electrons diffuse across the equatorial loss cone in less than a quarter of a bounce period and the electron distribution is close to isotropic. This can happen in the plasma sheet but it is not the situation at distances close to Earth.

Electrons can be exposed the weak diffusion which does not result in their efficient depletion into the equatorial loss cone and the electron distribution is essentially anisotropic. Therefore, in addition to the considering the strong diffusion, we took into account the weak diffusion regime following [*Chen and Schulz*, 2001a; *Chen et al.*, 2005]. No types of waves the electrons interact with were specified. Addition of weak diffusion resulted in somewhat reasonable agreement between the observed and modeled fluxes at geostationary orbit, although the modeled fluxes are about one order of magnitude higher than the observed ones, mainly on the dayside. The fluxes with electron energies from 15 to 50 keV are better modeled. Inside geostationary orbit, the evolution of the modeled fluxes during the storm is rather close to the observed features. Detailed dynamics of the observed fluxes is not reproduced. *Chen et al.* [2015] used the same combination of models for strong and weak diffusion regimes for the August 10, 2000 storm event modeling. Their comparison was mostly qualitative, since they showed only one energy-time color spectrogram and did not compare electron fluxes in specific energy ranges in details. Instead, all the comparison was done by eye inspection of the observed and modeled spectrograms. The conclusion which was reached was that the observed fluxes were overestimated on the morning and dayside.

When the electron losses due to interactions with specific types of waves, such as chorus waves [*Orlova and Shprits*, 2014] and with hiss waves [*Orlova et al.*, 2014, 2016] are introduced, the observed geostationary electron fluxes are very well reproduced during the storm maximum. The fluxes of electrons with energies from 15 to 50 keV are closer to the observed ones than those with lower energies between 5 and 15 keV. The discrepancy between the modeled and the observed fluxes is rather pronounced (reaching even 2 orders of magnitude difference, especially for lower energies) during the first and last day of the modeled storm. The way how the electron lifetimes were parameterized for low energies with the same coefficients for all Kp values and for wide energy range may be the reason of the disagreement between the modeled and the observed fluxes. Moreover, the simple combination of the electron lifetimes due to chorus and hiss waves has non-smooth transitions between them at the location where lifetime due to chorus goes into the lifetime due to hiss. In addition, transitions between MLT-sectors inside both models are also with some jumps. This also can lead to rather complicated behavior or modeled fluxes. Several details in the dynamics of the observed fluxes are missing. The combination of models for chorus waves [*Orlova and Shprits*, 2014] and for hiss waves [*Orlova et al.*, 2014] was used in the study of *Chen et al*. [2015]. As was mentioned above, their qualitative analysis of the model performance was based on the eye inspection of one energy-time spectrogram. The conclusion they stated was that the major features of that spectrogram were reproduced reasonably well which is difficult to quatify. It was also mentioned that the lack of specification of the scattering rates in the 1500-2100 MLT sector can be the reason of discreapancy betweet the modeled and observed fluxes.

The presented paper is the first effort to validate the IMPTAM at and inside geostationary model simultaneously. Although, the detailed dynamics of observed fluxes was not fully reproduced, the representation for electron lifetimes for keV electrons obtained from the VERB code is the best available model at present. The keV electron fluxes vary significantly on the time scales of tens of minutes. The electron lifetimes parameterized by 3-hour Kp index do not reflect the full picture of shorter time variations. Further IMPTAM validation will lead to better understanding of the necessity to develop the model for electron lifetimes with more detailed dependence on energy and other than Kp geomagnetic indices.

Keeping in mind the points discussed above, the conclusions are the followings:

1. All the variations of the modeled electron fluxes at geostationary orbit are caused by the changes in IMPTAM's parameters, namely, the solar wind and IMF parameters and Dst index included in background magnetic and electric field models and boundary conditions, if no electron loss processes are considered.

2. If the electron losses are represented by the strong diffusion limit everywhere in the inner magnetosphere, the modeled electron fluxes drop to almost zero values on the day- and duskside. The non-zero fluxes on the nightside are due to fresh electrons coming from the model boundary.

3. Addition of weak diffusion to the strong diffusion regime results in rather reasonable agreement between the variations of the observed and modeled fluxes at geostationary orbit. At the same time, the modeled fluxes are about one order of magnitude higher than the observed ones on the dayside. Inside geostationary orbit, the evolution of the modeled fluxes during the storm is rather close to the observed features.

4. With electron losses due to interactions with specific types of waves, such as chorus and hiss introduced, the observed geostationary electron fluxes at the storm maximum

are very well reproduced. The fluxes of electrons with energies from 15 to 50 keV are closer to the observed ones than those with lower energies between 5 and 15 keV. The discrepancies between the modeled and the observed fluxes can be attributed to the parameterization of electron lifetimes for low energies with the same coefficients for all Kp values, to the non-smooth transitions between lifetimes due to chorus and hiss, and the lifetime jumps between MLT-sectors.

5. IMPTAM is a powerful tool for modeling keV electron fluxes at different distances in the inner Earth's magnetosphere.

Acknowledgments

The projects leading to these results have received funding from the European Union Seventh Framework Programme (FP7/2007-2013) under grant agreement No 606716 SPACESTORM and from the European Union's Horizon 2020 research and innovation program under grant agreement No 637302 PROGRESS. N. Ganushkina thanks the International Space Science Institute in Bern, Switzerland, for their support of the international teams on "Analysis of Cluster Inner Magnetosphere Campaign data, in application of the dynamics of waves and wave-particle interaction within the outer radiation belt" and "Ring current modeling: Uncommon Assumptions and Common Misconceptions".

References

Agapitov, O., A. Artemyev, V. Krasnoselskikh, Y. V. Khotyaintsev, D. Mourenas, H. Breuillard, M. Balikhin, and G. Rolland (2013), Statistics of whistler-mode waves in the outer radiation belt: Cluster STAFF-SA measurements, J. Geophys. Res. Space Physics, 118, 3407-3420, doi:10.1002/jgra.50312.

Albert, J. M. (1994), Quasi-linear pitch angle diffusion coefficients: Retaining high harmonics, J. Geophys. Res., 99(A12), 23,741-23,745, doi:10.1029/94JA02345.

Albert, J. M. (2005), Evaluation of quasi-linear diffusion coefficients for whistler mode waves in a plasma with arbitrary density ratio, J. Geophys. Res., 110, A03218, doi:10.1029/2004JA010844.

Albert, J. M., and Y. Y. Shprits (2009), Estimates of lifetimes against pitch angle diffusion, J. Atmos. Sol. Terr. Phys., 71, 1647-1652, doi:10.1016/ j.jastp.2008.07.004.

Artemyev, A. V., D. Mourenas, O. V. Agapitov, and V. V. Krasnoselskikh (2013a), Parametric validations of analytical lifetime estimates for radiation belt electron diffusion by whistler waves, Ann. Geophys., 31, 599-624, doi:10.5194/angeo-31-599-2013.

Artemyev, A. V., O. V. Agapitov, D. Mourenas, V. Krasnoselskikh, and L. M. Zelenyi (2013b), Storm-induced energization of radiation belt electrons: Effect of wave obliquity, Geophys. Res. Lett., 40, 4138-4143, doi:10.1002/grl.50837.

Bame, S. J., McComas, D. J., Thomsen, M. F., et al. (1993), Magnetospheric Plasma Analyzer for Spacecraft with Constrained Resources, *Rev. Sci. Instr.*, *64*, 1026.

Belian, R. D., G. R. Gisler, T. Cayton, and R. Christensen (1992), High-Z energetic particles at geosynchronous orbit during the great solar proton event series of October 1989, *J. Geophys. Res.*, *97*, 16,897.

Blake, J. B., et al. (2013), The Magnetic Electron Ion Spectrometer (MagEIS) instruments aboard the Radiation Belt Storm Probes (RBSP) spacecraft, Space Sci. Rev., 179, 383-421, doi:10.1007/s11214-013-9991-8.

Boyle, C., Reiff, P., and Hairston, M., Empirical polar cap potentials, *J. Geophys. Res.*, *102(A1)*, 111-125.

Brautigam, D. H., and Albert, J. M. (2000). Radial diffusion analysis of outer radiation belt electrons during the 9 October 1990 magnetic storm. *J*. Geophys. Res., *1*05, 291.

Buchner, J. and Zelenyi, L. M.: Chaotization of the electron motion as the cause of an internal magnetotail instability and substorm onset, J. Geophys. Res., 92, 13456-13466, 1987.

Bunch, N. L., M. Spasojevic, and Y. Y. Shprits (2012), Off-equatorial chorus occurrence and wave amplitude distributions as observed by the Polar Plasma Wave Instrument, J. Geophys. Res., 117, A04205, doi:10.1029/2011JA017228.

Bunch, N. L., M. Spasojevic, Y. Y. Shprits, X. Gu, and F. Foust (2013), The spectral extent of chorus in the off-equatorial magnetosphere, J. Geophys. Res. Space Physics, 118, 1700-1705, doi:10.1029/2012JA018182.

Chen, M. W., and M. Schulz (2001a), Simulations of diffuse aurora with plasma sheet electrons in pitch angle diffusion less than everywhere strong, J. Geophys. Res., 106(A12), 28,949-28,966, doi:10.1029/2001JA000138.

Chen, M. W., and M. Schulz, Simulations of storm time diffuse aurora with plasmas heete lectronsin strongp itch angled iffusion, J. GeophysR. es., 106, 1873-1886, 2001b.

Chen, M. W., M. Schulz, P. C. Anderson, G. Lu, G. Germany, and M. WÃijest (2005), Storm time distributions of diffuse auroral electron energy and X-ray flux: Comparison of drift-loss simulations with observations, J. Geophys. Res., 110, A03210, doi:10.1029/2004JA010725.

Chen, Y, G. D. Reeves, and R. H. W. Friedel, The energization of relativistic electrons in the outer Van Allen radiation belt, Nature Physics, doi:10.1038/nphys655, 2007.

Chen, M. W., C. L. Lemon, K. Orlova, Y. Shprits, J. Hecht, and R. L.Walterscheid (2015), Comparison of simulated and observed trapped and precipitating electron fluxes during a magnetic storm, Geophys. Res. Lett., 42, 8302-8311, doi:10.1002/2015GL065737.

Christon, S. P., D. J. Williams, D. G. Mitchell, L. A. Frank, and C. Y. Huang, Spectral characteristics of plasma sheet ion and electron populations during undisturbed geomagnetic conditions, J. Geophys. Res., 94(A10), 13,409-13,424, doi:10.1029/JA094iA10p13409, 1989.

Christon, S. P., D. J. Williams, D. G. Mitchell, C. Y. Huang, and L. A. Frank, Spectral characteristics of plasma sheet ion and electron populations during disturbed geomagnetic conditions, J. Geophys. Res., 96, 1, doi:10.1029/90JA01633, 1991.

Davis, V. A., M. J. Mandell, and M. F. Thomsen, Representation of the measured geosynchronous plasma environment in spacecraft charging calculations, J. Geophys. Res., 113, A10204, doi:10.1029/2008JA013116, 2008.

Delcourt, D. C., Sauvaud, J.-A., Martin, Jr., R. F. and Moore, T. E.: On the nonadiabatic precipitation of ions from the near-earth plasma sheet, J. Geophys. Res., 101, 17409-17418, 1996.

Dichter, B. K., J. 0. McGarity, M. R. Oberhardt, V. T. Jordanov, D. J. Sperry, A. C. Huber, J. A. Pantazis, E. G. Mullen, G. Ginet, and M. S. Gussenhoven (1998), Compact Environmental Anomaly Sensor (CEASE): A Novel Spacecraft Instrument for In Situ Measurements of Environmental Conditions, *IEEE Trans. Nucl. Sci.*, *45*, 2758-2764.

Dubyagin, S., N. Y. Ganushkina,I. SillanpÃď'Ãď', and A. Runov, Solar wind-driven variations of electron plasma sheet densities and temperatures beyond geostationary orbit during storm times, J. Geophys. Res. Space Physics, 121, doi:10.1002/2016JA022947, 2016.

Fok, M.-C., et al., Global ENA IMAGE observations, Space Sci. Rev., 109, 77-103, 2003.

L.A. Frank, Several observations of low-energy protons and electrons in the Earth's magnetosphere with OGO 3. J. Geophys. Res., **72(7)**, 1905-1916, doi:10.1029/JZ072i007p01905 (1967).

Funsten, H. O., et al., Helium, Oxygen, Proton, and Electron (HOPE) Mass Spectrometer for the Radiation Belt Storm Probes Mission, Space Science Reviews, doi:10.1007/s11214-013-9968-7, 2013

Fälthammar, C.-G. (1965), Effects of time-dependent electric fields on geomagnetically trapped radiation, *J*. Geophys. Res., *7*0, 2503.

Hanser, F. A., EPS/HEPAD calibration and data handbook, Tech. Rep. GOESN-ENG-048D, Assurance Technology Corporation, Carlisle, Mass., 2011 [Available at http://www.ngdc.noaa.gov/stp/satellite/goes/documentation.html]

Haque, N., M. Spasojevic, O. Santolik, and U. S. Inan (2010), Wave normal angles of magnetospheric chorus emissions observed on the Polar spacecraft, J. Geophys. Res., 115, A00F07, doi:10.1029/2009JA014717.

Helliwell, R. A. (1967), A theory of discrete VLF emissions from the magnetosphere, J. Geophys. Res., , 72, 4773-4790, doi:10.1029/JZ072i019p04773.

Horne, R. B., R. M. Thorne, Y. Y. Shprits, N. P. Meredith, S. A. Glauert, A. J. Smith, S. G. Kanekal, D. N. Baker, M. J. Engebretson, J. L. Posch, M. Spasojevic, U. S. Inan, J. S. Pickett, and P. M. E. Decreau (2005), Wave acceleration of electrons in the Van Allen radiation belts, Nature, 437, 227-230, doi:10.1038/nature03939.

Horne, R. B., et al., Forecasting the EarthâĂŹs electrons radiation belts and modeling solar energetic particle events: Recent results from SPACECAST, J. Space Weather Space Clim., 3, A20, doi:10.1051/swsc/2013042, 2013.

Gabrielse, C., V. Angelopoulos, A. Runov, and D. L. Turner, The effects of transient, localized electric fields on equatorial electron acceleration and transport toward the inner magnetosphere, J. Geophys. Res., 117, A10213, doi:10.1029/2012JA017873, 2012.

Gabrielse, C., V. Angelopoulos, A. Runov, and D. L. Turner, Statistical characteristics of particle injections throughout the equatorial magnetotail, J. Geophys. Res. Space Physics, 119, 2512-2535, doi:10.1002/2013JA019638, 2014.

Ganushkina, N. Yu., T. I. Pulkkinen, T. Fritz (2005), Role of substorm-associated impulsive electric fields in the ring current development during storms, *A*nn. Geophys., *2*3, 579-591.

Ganushkina N. Yu., O. Amariutei, Y. Y. Shpritz, and M. Liemohn (2013), Transport of the plasma sheet electrons to the geostationary distances, *J*. Geophys. Res., *118*, doi:10.1029/2012JA017923.

Ganushkina N. Yu., M. Liemohn, O. Amariutei, and D. Pitchford (2014), Low energy electrons (5-50 keV) in the inner magnetosphere, *J*. Geophys. Res., 119, 246-259, doi:10.1002/2013JA019304.

Ganushkina N. Yu., O. A. Amariutei, D. Welling, and D. Heynderickx, (2015), Nowcast model for low-energy electrons in the inner magnetosphere, *S*pace Weather, 13, doi:10.1002/2014SW001098.

Garrett, H. B., The charging of spacecraft surfaces, Rev. Geophys., 1 9(4), 577, doi:10.1029/RG019i004p00577, 1981.

Glauert, S. A., and R. B. Horne (2005), Calculation of pitch angle and energy diffusion coefficients with the PADIE code, J. Geophys. Res., 110, A04206, doi:10.1029/2004JA010851.

Golden, D. I., M. Spasojevic,W. Li, and Y. Nishimura (2012), Statistical modeling of plasmaspheric hiss amplitude using solar wind measurements and geomagnetic indices, Geophys. Res. Lett., 39, L06103, doi:10.1029/2012GL051185

Gu, X., Y. Y. Shprits, and B. Ni (2012), Parameterized lifetime of radiation belt electrons interacting with lower-band and upper-band oblique chorus waves, Geophys. Res. Lett., 39, L15102, doi:10.1029/2012GL052519.

Jordanova, V. K., J. Albert, and Y. Miyoshi, Relativistic electron precipitation by EMIC waves from self-consistent global simulations, J. Geophys. Res., 113, A00A10, doi:10.1029/2008JA013239, 2008.

Kennel, C. F. (1969), Consequences of a magnetospheric plasma, Rev. Geophys., 7(1,2), 379âĂŞ419, doi:10.1029/RG007i001p00379.

Kennel, C. F., and H. E. Petschek (1966), Limit on Stably Trapped Particle Fluxes, J. Geophys. Res., , 71, 1.

Lanzerotti, L. J., K. LaFleur, C. G. Maclennan, and D. W. Maurer (1998), Geosynchronous spacecraft charging in January 1997, Geophys. Res. Lett., 25(15), 2967-2970.

Lemon, C., R. Wolf, T. W. Hill, and S. Sazykin (2004), Magnetic storm ring current injection modeled with the rice convection model and a self-consistent magnetic field, Geophys. Res. Lett., 31, L21801, doi:10.1029/2004GL020914.

Li, X., Baker, D. N., Temerin, M. et al.,Simulation of dispersionless injections and drift echoes of energetic electrons associated with substorms (1998), *G*eophys. Res. Lett., 25, 3763-3766.

Li, W., J. Bortnik, R. M. Thorne, and V. Angelopoulos (2011), Global distribution of wave amplitudes and wave normal angles of chorus waves using THEMIS wave observations, J. Geophys. Res., 116, A12205, doi:10.1029/2011JA017035.

Li, W., Q. Ma, R. M. Thorne, J. Bortnik, C. A. Kletzing, W. S. Kurth, G. B. Hospodarsky, and Y. Nishimura (2015), Statistical properties of plasmaspheric hiss derived from Van Allen Probes data and their effects on radiation belt electron dynamics, J. Geophys. Res. Space Physics, 120, 3393-3405, doi:10.1002/2015JA021048.

Liemohn, M. W., and P. C. Brandt, Small-scale structure in the stormtime ring current, in Inner Magnetosphere Interactions: New Perspectives From Imaging, Geophys. Monogr. Ser., vol. 159, edited by J. L. Burch, M. Schulz, and H. Spence, p. 167, AGU, Washington, D. C, 2005.

Lichtenberg, A. J., and M. A. Lieberman (1983), Regular and Stochastic Motion, Springer, New York.

Liu, S., M. W. Chen, J. L. Roeder, L. R. Lyons, and M. Schulz (2005), Relative contribution of electrons to the stormtime total ring current energy content, Geophys. Res. Lett., 32, L03110, doi:10.1029/2004GL021672.

Lyons, L. R., R. M. Thorne, and C. F. Kennel (1972), Pitch-angle diffusion of radiation belt electrons within the plasmasphere, J. Geophys. Res., 77, 3455-3474, doi:10.1029/JA077i019p03455.

Lyons, L. R., and R. M. Thorne (1973), Equilibrium structure of radiation belt electrons, J. Geophys. Res., 78(13), 2142âĂŞ2149, doi:10.1029/ JA078i013p02142.

Mauk, B. H., N. J. Fox, S. G. Kanekal, R. L. Kessel, D. G. Sibeck, and A. Ukhorskiy , Science objectives and rationale for the Radiation Belt Storm Probes mission, Space Sci.Rev., 179, doi: 10.1007/s11214-012-9908, 2013.

Meredith, N. P., R. B. Horne, R. M. Thorne, D. Summers, and R. R. Anderson (2004), Substorm dependence of plasmaspheric hiss, J. Geophys. Res., 109, A06209, doi:10.1029/2004JA010387.

Meredith, N. P., R. B. Horne, A. Sicard-Piet, D. Boscher, K. H. Yearby, W. Li, and R. M. Thorne (2012), Global model of lower band and upper band chorus from multiple satellite observations, J. Geophys. Res., 117, A10225, doi:10.1029/2012JA017978.

Mourenas, D., and J.-F. Ripoll (2012), Analytical estimates of quasi-linear diffusion coefficients and electron lifetimes in the inner radiation belt, J. Geophys. Res., 117, A01204, doi:10.1029/2011JA016985.

Mourenas, D., A. V. Artemyev, J.-F. Ripoll, O. V. Agapitov, and V. V. Krasnoselskikh (2012), Timescales for electron quasi-linear diffusion by parallel and oblique lower-band chorus waves, J. Geophys. Res., 117, A06234, doi:10.1029/2012JA017717.

Ni, B., R. M. Thorne, N. P. Meredith, Y. Y. Shprits, and R. B. Horne (2011), Diffuse auroral scattering by whistler mode chorus waves: Dependence on wave normal angle distribution, J. Geophys. Res., 116, A10207, doi:10.1029/2011JA016517.

Orlova, K., and Y. Shprits (2014), Model of lifetimes of the outer radiation belt electrons in a realistic magnetic field using realistic chorus wave parameters, *J*. Geophys. Res., *1*19, 770-780, doi:10.1002/2013JA019596.

Orlova, K., M. Spasojevic, and Y. Shprits (2014), Activity-dependent global model of electron loss inside the plasmasphere, Geophys. Res. Lett., 41, doi:10.1002/2014GL060100.

Orlova, K., Y. Shprits, and M. Spasojevic, New global loss model of energetic and relativistic electrons based on Van Allen Probes measurements, J. Geophys. Res. Space Physics, 121, 1308-1314, doi:10.1002/2015JA021878, 2016.

Roederer, J. G. (1970), Dynamics of geomagnetically trapped radiation, Springer-Verlag, New York, 36pp.

Rodriguez, J. V., GOES 13-15 MAGE/PD pitch angles, Algorithm Theoretical Basis Document, version 1.0 NOAA NESDIS NGDC, September 10, 2014 [Available at http://www.ngdc.noaa.gov/stp/satellite/goes/documentation.html]

Russell, C. T., R. E. Holzer, and E. J. Smith (1969), OGO 3 observations of ELF noise in the magnetosphere: 1. Spatial extent and frequency of occurrence, J. Geophys. Res., 74(3), 755-777, doi:10.1029/JA074i003p00755.

Sarris, T. E, Li, X., Tsaggas, N., and Paschalidis, N. (2002), Modeling energetic particle injections in dynamic pulse fields with varying propagation speeds, *J*. Geophys. Res., *1*07, 1033, doi: 10.1029/2001JA900166.

Schulz, M. (1974), Particle lifetimes in strong diffusion, Astrophys. Space Sci., 31, 37-42.

Schulz, M., and L. Lanzerotti (1974), Particle Diffusion in the Radiation Belts, Springer, New York.

Schulz, M. (1998), Particle drift and loss rates under strong pitch angle diffusion in Dungey's model magnetosphere, J. Geophys. Res., 103(A1), 61âĂŞ67, doi:10.1029/97JA02042.

Sergeev, V. A. and Tsyganenko, N. A.: Energetic particle losses and trapping boundaries as deduced from calculations with a realistic magnetic field model, Planet. Space Sci., 30, 999-1006, 1982.

Shprits Y. Y., and R. M. Thorne (2004), Time dependent radial diffusion modeling of relativistic electrons with realistic loss rates, *G*eophys. Res. Lett., *3*1, L08805, doi:10.1029/2004GL019591.

Shprits Y. Y., R. M. Thorne, R. B. Horne, D. Summers, Bounce-averaged diffusion coefficients for field-aligned chorus waves, J. Geophys. Res., 111, A10225, doi:10.1029/2006JA011725, 2006.

Shprits, Y. Y., N. P. Meredith, and R. M. Thorne (2007), Parameterization of radiation belt electron loss timescales due to interactions with chorus waves, Geophys. Res. Lett., 34, L11110, doi:10.1029/2006GL029050.

Shprits, Y. Y., et al., Review of modeling of losses and sources of relativistic electrons in the outer radiation belt: I. Radial transport, J. Atmos. Sol. Terr. Phys., 70(14), 1679-1693, 2008a.

Shprits, Y. Y., Review of modeling of losses and sources of relativistic electrons in the outer radiation belt: II. Local acceleration and loss, J. Atmos. Sol. Terr. Phys., 70(14), 1694-1713, 2008b.

Spasojevic, M., and Y. Y. Shprits (2013), Chorus functional dependencies derived from CRRES data, Geophys. Res. Lett., 40, 3793-3797, doi:10.1002/grl.50755.

Spasojevic, M., Y. Y. Shprits, and K. Orlova (2015), Global empirical models of plasmaspheric hiss using Van Allen Probes, J. Geophys. Res. Space Physics, 120, 10,370-10,383, doi:10.1002/2015JA021803

Spence, H. E., Reeves, G. D., Baker, D. N. et al., Science Goals and Overview of the Energetic Particle, Composition, and Thermal Plasma (ECT) Suite on NASA's Radiation Belt Storm Probes (RBSP) Mission, Space Science Reviews, 179: 311, doi:10.1007/s11214-013-0007-5, 2013.

Thorne, R. M., E. J. Smith, R. K. Burton, and R. E. Holzer (1973), Plasmaspheric hiss, J. Geophys. Res., 78(10), 1581-1596, doi:10.1029/ JA078i010p01581.

Thorne, R. M. (2010), Radiation belt dynamics: The importance of wave-particle interactions, Geophys. Res. Lett., , 37, L22107, doi:10.1029/2010GL044990.

Tsurutani, B. T., and E. J. Smith (1974), Postmidnight chorus: A substorm phenomenon, J. Geophys. Res., , 79, 118127, doi:10.1029/JA079i001p00118.